JGR Oceans

RESEARCH ARTICLE

10.1029/2023JC020844

Variability of Dissolved Organic Matter Sources in the Upper Eurasian Arctic Ocean

Xianyu Kong[1], Mats A. Granskog[2], Clara J. M. Hoppe[1], Allison A. Fong[1], Colin A. Stedmon[3], Sandra Tippenhauer[1], Adam Ulfsbo[4], Myriel Vredenborg[1], and Boris P. Koch[1,5]

[1]Alfred-Wegener-Institut Helmholtz Zentrum für Polar- und Meeresforschung, Bremerhaven, Germany, [2]Fram Centre, Norwegian Polar Institute, Tromsø, Norway, [3]National Institute of Aquatic Resources, Technical University of Denmark, Kongens Lyngby, Denmark, [4]Department of Marine Sciences, University of Gothenburg, Gothenburg, Sweden, [5]University of Applied Sciences, Bremerhaven, Germany

Abstract Chromophoric dissolved organic matter (CDOM) is a ubiquitous component in marine environments, and substantial changes in its sources and distribution, related to the carbon cycle in the Arctic Ocean, are expected due to Arctic warming. In this study, we present unique CDOM data in the Eurasian Arctic Ocean derived from the year-round MOSAiC expedition. We used CDOM absorbance spectra and fluorescence excitation-emission matrices in combination with parallel factor analysis to characterize differences in DOM sources and composition. Our results suggested that terrestrial DOM was less sensitive to seasonal changes but controlled by regionality in hydrography. Elevated dissolved organic carbon (DOC) levels in polar surface water were primarily derived from terrigenous sources as identified by CDOM absorption and fluorescence characteristics. In the Amundsen Basin and western Fram Strait surface waters, to which terrestrial DOM is primarily transported by the Transpolar Drift, we found, on average, a 188% larger meteoric water fraction and a 40% higher DOC concentration compared to the Atlantic water that dominated western Nansen Basin and Yermak Plateau. In the Amundsen Basin, the DOC concentration in summer of surface water was only 13% higher compared to winter season. Additionally, autochthonous DOM and chlorophyll-a concentrations were relatively low in surface water and exhibited significant differences compared to those observed in summer, while there were significant differences between autochthonous DOM and chlorophyll-a. We also observed that sea ice melt contributed to autochthonous DOM in summer, while storms in winter affected the vertical distribution of terrestrial and autochthonous DOM in the subsurface.

Plain Language Summary In the Arctic Ocean, dissolved organic matter (DOM) is important because it represents a large carbon reservoir that cycles through the environment and supports the growth of marine life in the Arctic. DOM originates from various sources and its composition changes depending on factors like location and time of year, largely influenced by ocean currents. Microbes in the water break down DOM, but this process is hindered during the winter months and in areas with limited sunlight. Due to the very limited and challenging accessibility of the Central Arctic Ocean, there is a lack of DOM data, especially during winter in the Eurasian Arctic Ocean. Scientists conducted a comprehensive year-round study during the MOSAiC expedition and discovered that much of the DOM in the Arctic comes from land in Siberia. Additionally, seasonal changes were observed to alter the composition of locally produced chromophoric DOM (CDOM) in surface waters of the Amundsen Basin. In contrast, terrestrial CDOM is less responsive to seasonal shifts but more influenced by regional variations in hydrography. This highlights the substantial role of regional hydrographic differences in shaping the characteristics of DOM in surface water across the Eurasian Arctic Ocean.

Key Points:

- Elevated dissolved organic carbon levels in polar surface water are primarily derived from terrigenous sources in the Eurasian basin
- Contrasting dissolved organic matter characteristics in Amundsen and Nansen basins caused by Transpolar Drift waters
- Autochthonous dissolved organic matter in polar surface water is low in winter and significantly different from that in summer

Supporting Information:

Supporting Information may be found in the online version of this article.

Correspondence to:

X. Kong,
xianyu.kong@awi.de

Citation:

Kong, X., Granskog, M. A., Hoppe, C. J. M., Fong, A. A., Stedmon, C. A., Tippenhauer, S., et al. (2024). Variability of dissolved organic matter sources in the upper Eurasian Arctic Ocean. *Journal of Geophysical Research: Oceans*, *129*, e2023JC020844. https://doi.org/10.1029/2023JC020844

Received 21 DEC 2023
Accepted 13 JUN 2024

Author Contributions:

Conceptualization: Xianyu Kong, Mats A. Granskog, Colin A. Stedmon, Boris P. Koch
Data curation: Xianyu Kong, Boris P. Koch
Formal analysis: Xianyu Kong
Investigation: Xianyu Kong, Mats A. Granskog, Clara J. M. Hoppe, Allison A. Fong, Colin A. Stedmon, Sandra Tippenhauer, Adam Ulfsbo, Myriel Vredenborg, Boris P. Koch
Methodology: Xianyu Kong, Boris P. Koch
Resources: Mats A. Granskog, Boris P. Koch
Supervision: Boris P. Koch

1. Introduction

Dissolved organic matter (DOM) constitutes the largest pool of organic material in the ocean (Hansell et al., 2009). It is a complex mixture of allochthonous (terrestrially derived) and autochthonous (in situ biological production) materials (Stedmon et al., 2007) and plays a crucial role in the global carbon cycle, rivaling the atmospheric CO_2 content in scale (Friedlingstein et al., 2022). DOM attenuates the penetration of ultraviolet (UV) and visible light (Hill, 2008; Morris et al., 1995), serves as an energy and nutrient source for heterotrophic communities (Wetzel, 1984), and acts as a trace metal ligand (Hirose, 2007). In the Arctic, the distribution and

Visualization: Xianyu Kong, Mats A. Granskog, Boris P. Koch
Writing – original draft: Xianyu Kong
Writing – review & editing: Xianyu Kong, Mats A. Granskog, Clara J. M. Hoppe, Allison A. Fong, Colin A. Stedmon, Sandra Tippenhauer, Adam Ulfsbo, Myriel Vredenborg, Boris P. Koch

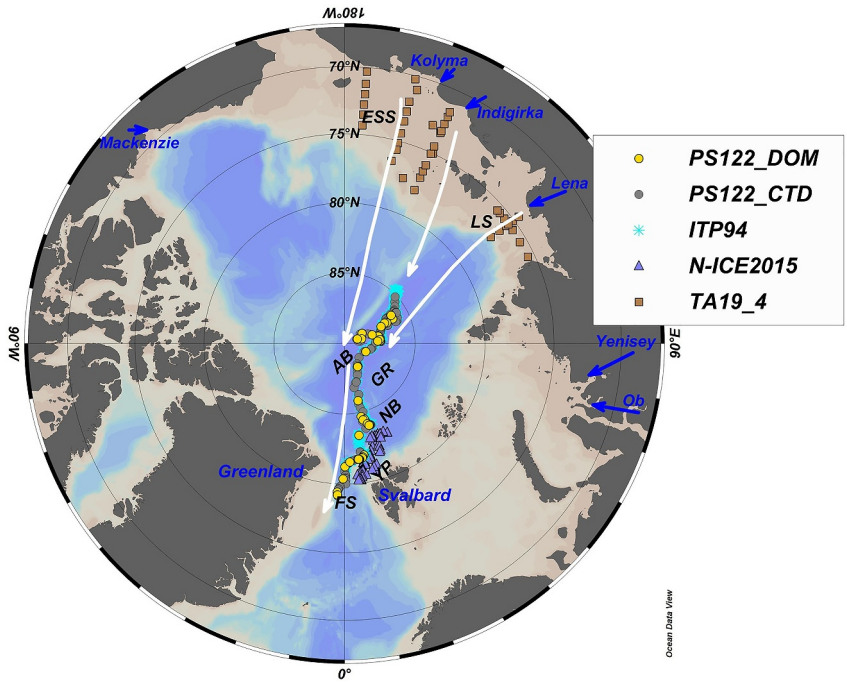

Figure 1. Map of the study area. Dots represent the CTD stations conducted during the MOSAiC expedition. Stations where DOM samples were collected from the CTD rosette are highlighted in yellow. Triangles represent stations of the N-ICE2015 expedition. Squares represent stations of the TA19_4 expedition. Magenta asterisks represent profiles taken by ITP94. AB: Amundsen Basin, GR: Gakkel Ridge, NB: western Nansen Basin, YP: Yermak Plateau, and FS: Fram Strait. Blue arrows indicate major Arctic River inflows. White arrows indicate the approximate location of the TPD. Note that the Arctic Oscillation (Macdonald et al., 2005) can result in a substantial interannual spatial variability of the location of the TPD.

dynamics of DOM have attracted much attention in recent decades. Studies have shown that the land-ocean flux of DOM to the Arctic Ocean has increased due to climate warming and permafrost thawing (Frey & Smith, 2005; O'Donnell et al., 2016; Spencer et al., 2015). The fraction of DOM that absorbs light within the UV and visible spectrum is known as chromophoric dissolved organic matter (CDOM). CDOM is optically active and ubiquitous in the Arctic Ocean, where it has a significant impact on the penetration of UV radiation, solar heating of surface waters, and light availability for primary production (Granskog et al., 2007; Hill, 2008; Pegau, 2002). Optical spectroscopy (absorbance and fluorescence) is widely used to characterize the properties and dynamics of CDOM (Baker & Spencer, 2004; Guéguen et al., 2015; Parlanti et al., 2000; Stedmon et al., 2021; Yamashita & Jaffé, 2008). Fluorescence excitation emission matrices (EEMs) analyzed using parallel factor analysis (PARAFAC) have been widely used to identify the major components of the fluorescent dissolved organic matter (FDOM), a subfraction of CDOM that emits a fraction of the absorbed energy as fluorescence (Murphy et al., 2008; Stedmon et al., 2003).

The upper Eurasian/Eastern Arctic Ocean generally consists of three distinct layers: polar surface water (PSW), the halocline layer, and the Atlantic Water (AW) layer beneath the halocline (Rudels et al., 1996). PSW is characterized by relatively low salinity and cold temperatures, while in the halocline layer salinity increases rapidly with depth, separating surface waters from the relatively warm and saline AW layer beneath. The major suppliers of freshwater to the Arctic Ocean are low-salinity Pacific Water entering through the Bering Strait, precipitation over the Arctic region, continental runoff, and sea ice meltwater (Rudels, 1989; Rudels et al., 1996). River discharge, in particular, brings high loads of terrestrial organic matter into the Arctic surface waters and upper halocline (Bélanger et al., 2006; Stedmon et al., 2011). The Transpolar Drift (TPD; Figure 1) is the major surface current in the eastern Arctic Ocean that transports sea ice and shelf waters from the Laptev and East Siberian Seas across the Arctic Ocean towards the Fram Strait (Charette et al., 2020). The TPD carries a large amount of freshwater and terrestrially derived DOM, indicated by elevated CDOM concentrations (Slagter et al., 2017) and relatively low salinities in PSW (e.g., Paffrath et al., 2021). The position of the TPD varies with the Arctic Oscillation (Charette et al., 2020; Mauritzen, 2012; Mysak, 2001) affecting the local CDOM

concentration. CDOM is also influenced by seasonal changes of the Arctic River freshwater discharge, which is lowest in winter (Mann et al., 2016; Spencer et al., 2008). In the central Arctic Ocean, sea ice meltwater can also introduce freshwater into the surface layer in summer. In winter, brine released by freezing, increases the density of the surface layer (Jones et al., 2008). Hence, PSW can be homogenized by convective mixing and brine rejection during the seasonal ice formation and re-stratified during the sea ice melt (Korhonen et al., 2013; Rudels, 1989; Rudels et al., 2004). In addition to physical processes, primary production and heterotrophic consumption in the Arctic Ocean contribute to the distribution of DOM in surface waters (Hach et al., 2020; Mathis et al., 2007). The Arctic experiences significant spatial and temporal variability in solar radiation, sea ice extent, and nutrient availability, leading to considerable differences in primary production (Tremblay & Gagnon, 2009). This also affect the production and release of bioavailable DOM, a source of carbon and energy for heterotrophic bacteria and sustaining the structure microbial food webs (Carlson & Hansell, 2015). Especially during the Arctic winter with its polar night and extreme low temperature, reduced primary productivity (Terhaar et al., 2021), decreased heterotrophic bacteria activity (Sherr & Sherr, 2003), and limited photodegradation (Stedmon et al., 2011) could significantly influence the dynamics of DOM, and may lead to the accumulation of DOM in PSW. The DOM in PSW is subsequently exported to the deep ocean through vertical mixing and overturning circulation, and gradually mineralized by microorganisms (Hansell & Carlson, 2001). In addition, strong tidal induced vertical mixing in winter could also affect the transport of DOM into deep waters (Pavlov, Stedmon, et al., 2016). While a previous study mentions the seasonality of CDOM in the Amerasian sector of the Arctic Ocean (Matsuoka et al., 2011), there is a lack of DOM measurements, especially during winter in the Eurasian sector (Boles et al., 2020; Gonçalves-Araujo et al., 2018).

The "Multidisciplinary Drifting Observatory for the Study of Arctic Climate" (MOSAiC) campaign involved a year-round (October 2019–September 2020) passive drift with sea ice of the RV Polarstern across the Eurasian Basin (Rabe et al., 2022). In this study, we present the first comprehensive year-round observations of DOM characteristics in the upper Eurasian Basin, and investigate how optical properties vary across the different water masses, regions and seasons. Our objective was to determine the spatial and temporal variability of the DOM composition and sources along the MOSAiC drift, and identify the dominant patterns driving the optical variability within PSW.

2. Materials and Methods

2.1. Study Area, Sampling, and In Situ Observation

DOM samples from seawater (sampling depth ranged from surface (~2 m) to bottom (~4,400 m)) were collected from the conductivity-temperature-depth (CTD) rosettes on the Central Observatory ice floe (Ocean City) and on RV Polarstern (Knust, 2017) during the expedition PS122 (MOSAiC). The vessel drifted with the first ice floe in the Amundsen Basin in October 2019 and crossed the Gakkel Ridge from March 18 to April 9, 2020. The drift continued through the Nansen Basin and reached the Yermak Plateau on 2 June 2020. After crossing the plateau, the drift entered the Fram Strait on 16 July 2020. After steaming back to the Amundsen Basin near the North Pole, RV Polarstern drifted again with a second ice floe from August 21 to September 18, 2020. Prior to analysis, seawater samples were filtered through pre-combusted (450°C, 5 hr) glass fiber filters (Whatman; GF/F). The 60 mL filtered water column samples were stored in acid washed high density polyethylene bottles at −20°C for dissolved organic carbon (DOC) and total dissolved nitrogen (TDN; sum of dissolved inorganic and organic components) measurements. Samples from November 2019 to February 2020 were also used for absorbance and EEMs measurements at the AWI Basic Laboratory. The 40 mL filtered water column samples from January 2020 to September 2020 were stored in pre-combusted amber glass vials at 4°C prior to absorbance and EEMs measurements at the AWI Basic Laboratory.

DOM samples from lead waters were collected in the Amundsen Basin using a peristaltic pump (Masterflex E/S portable sampler) from the surface down to 1 m between August 25 and September 4, 2020. These samples were filtered through an in-line 0.2 µm pore size Sterivex cartridge filter (polyethersulfone membrane) and stored in acid washed high density polyethylene bottles at −20°C for DOC and TDN measurements, and in pre-combusted amber glass vials at 4°C for absorbance and EEMs measurements. Salinity for lead water samples was measured with a hand-held multi-parameter probe (Cond 340i, WTW).

Chlorophyll-a (Chl-a) samples were collected from the two CTD rosettes roughly once per week from end of October 2019 to beginning of October 2020. 2–4 L of water were filtered onto precombusted GF/F filters (nominal pore size 0.7 μm) under gentle vacuum and frozen at −80°C.

The stable oxygen isotope ratio ($\delta^{18}O$) of underway seawater samples from underneath the research vessel and corresponding salinity used in this study was acquired from the PANGAEA data repository (Mellat et al., 2022).

The ice-tethered buoy ITP94 (Figure 1; Krishfield et al., 2008; Toole et al., 2011) was equipped with a fluorescence sensor and deployed on a 0.7-m-thick ice floe in collaboration with the MOSAiC expedition from RV Akademik Federov. This deployment involved conducting a full one-way profile every 1.5 days at depths between 7 and 760 m from October 2019 to July 2020. The in situ fluorescence signal, represented by the voltage output at excitation 370 nm and emission 460 nm from the fluorescence sensor (ECO FLbb-CD; WET Labs Inc.), firstly underwent a smoothing process using a moving average algorithm with a 20-m window. The fluorescence data was examined for drift or baseline bias by plotting the mean and standard deviation of each profile (see details in Stedmon et al., 2021). Subsequently, the voltage signal was linearly calibrated to represent DOM fluorescence in Raman units (see Figure S1 in Stedmon et al., 2021). We compared the results of the MOSAiC campaign with previous observations, CDOM absorption and fluorescence acquired during the Norwegian young sea ICE (N-ICE2015) expedition in the western Nansen Basin and Yermak Plateau (Figure 1; January–June 2015; Granskog et al., 2018), and data from the Laptev Sea and East Siberian Sea acquired during the TA19_4 expedition (Figure 1; September–October 2019; Hölemann et al., 2021).

2.2. Water Masses

During MOSAiC, vertical profiles of hydrographic data were collected with two CTD-systems operated on the Central Observatory ice floe (Ocean City, Tippenhauer et al., 2023a, 2023c) and on RV Polarstern (Tippenhauer et al., 2023b, 2023d). Six distinct water masses (Table S1 in Supporting Information S1) were identified along the drift track based on profiles of potential temperature (θ) and practical salinity (S_p) (Korhonen et al., 2013) Due to the comparatively low number of observations, the Deep Water (DW) category was not further classified into different water masses in this study (Meyer et al., 2017; Rudels, 2009; Smethie et al., 1988). More about the different water masses present during MOSAiC can be found in Schulz et al. (2023). Additionally, PSW samples from the NICE2015 and TA19-4 expeditions were compared with PSW samples collected during MOSAiC.

The water mass composition of surface waters during MOSAiC was determined using a three-endmember mass balance following the approach of Östlund and Hut (1984), defined by the following equations:

$$f_{aw} + f_{mw} + f_{sim} = 1 \quad (1)$$

$$f_{aw}S_{aw} + f_{mw}S_{mw} + f_{sim}S_{sim} = S \quad (2)$$

$$f_{aw}\delta_{aw} + f_{mw}\delta_{mw} + f_{sim}\delta_{sim} = \delta \quad (3)$$

where f is a water fraction, S is practical salinity, δ is $\delta^{18}O$, and the subscripts aw, mw, and sim represent Atlantic water, meteoric water (i.e., river runoff and precipitation), and sea ice melt water, respectively. Pacific Water was not used as a water source in this calculation, because there was no influence of Pacific Water within our sampling area (Paffrath et al., 2021; Schulz et al., 2023). Salinity and $\delta^{18}O$ endmember values were defined by following previous studies (Bauch et al., 2009; Granskog et al., 2012; Stedmon et al., 2015; Östlund & Hut, 1984), where S_{aw}, S_{mw}, S_{sim} were assigned to 34.92, 0, and 4, respectively, and δ_{aw}, δ_{mw} and δ_{sim} were assigned as 0.3, −20, and −2‰ respectively. A negative value for f_{sim} represents the amount of water removed by sea ice formation, and subsequent addition of brines (Bauch et al., 2009; Östlund & Hut, 1984).

2.3. Seasonal Transitions

Seasonal transitions during MOSAiC were defined by Shupe et al. (2022) based on daily averaged near-surface air temperature (2 m). At the beginning of the drift, the autumn freeze-up already started, with temperatures around −10°C. Subsequently, temperatures continued to decrease, with lows approaching −40°C. From the end of November 2019 to mid-April 2020, temperatures were generally below −20°C, which was defined as the winter season. In mid-April, there was an abrupt shift to temperatures above −20°C, coinciding with a southerly

advection event, marking the start of the spring season. In late May, the sea ice reached a consistent surface melt until early September, with temperatures limited to a narrow range of a few degrees around 0°C, defined as the summer melt season. From early September, the autumn freeze-up began again.

2.4. DOC and TDN Analysis

DOC and TDN were determined by high temperature catalytic oxidation (HTCO) and non-dispersive infrared spectroscopy and chemiluminescence detection with potassium hydrogen phthalate (PHP) and potassium nitrate (KNO_3) as standards, respectively (TOC-VCPN, Shimadzu; for details see e.g., Ksionzek et al., 2018). Samples were first poured into well-rinsed vials and acidified with 0.1 M HCl (Suprapur Merck) in the autosampler. Oxygen was then sparged into the samples for 5 min to remove inorganic carbon before 50 µL sample volume was injected directly on the catalyst at 680°C. The CO_2 generated was detected using an infrared detector, with a limit of determination of 7 µmol DOC kg^{-1} and a precision of ±5%. TDN was quantified by a chemiluminescence detector, with a limit of determination of 3 µmol TDN kg^{-1}.

2.5. Optical Spectroscopy

EEMs were measured using a spectrofluorometer (Aqualog, Horiba) equipped with a charge-coupled device (CCD) detector. Excitation wavelengths were scanned from 240 to 600 nm at 3 nm increments, while emissions were recorded from 220 to 620 nm at ∼3.3 nm increments. CDOM absorbance spectra were acquired using a spectrophotometer (UV2700, Shimadzu) in a quartz cuvette with an optical path length of 10 cm in the spectral range of 200–800 nm. EEMs and CDOM absorbance spectra were processed using the staRdom package in R studio (Version 3.5.1; Pucher et al., 2019). The fluorescence spectra were blank-corrected using ultrapure water (Milli-Q, Millipore), and then underwent inner filter effect correction and Raman normalization by dividing by the Raman peak of ultrapure water at an integrated excitation of 350 nm and an emission between 371 and 428 nm (Raman Units (R.U.); Lawaetz & Stedmon, 2009). A PARAFAC was then applied for all DOM samples (MOSAiC, N-ICE2015, and TA19_4 expeditions) to decompose the EEMs into different underlying fluorescent components (Murphy et al., 2008; Stedmon et al., 2003). The appropriate number of components was determined by a split-half validation (Murphy et al., 2013), for which the whole data set was split into six separate randomly split subsets. Tucker congruence coefficient (TCC) was used to assess the spectral similarity between components derived from different subsets (Wünsch et al., 2019), resulting in a four-component model ($TCC_{ex,em} > 0.99$; Figure S1 in Supporting Information S1). The four underlying components were named as C470, C400, C340, and C320 based on their fluorescence emission maxima (Figure 2). C470 is often assigned as humic-like components with terrestrial origin based on fluorescence maxima (Coble, 1996; Gonçalves-Araujo et al., 2016; Murphy et al., 2011). C400 has been assigned as humic-like substance with marine and microbial origin (Brogi et al., 2019; Coble, 1996; Wagner et al., 2015), or with terrestrial origin (Gonçalves-Araujo et al., 2016; Lin & Guo, 2020). In this study, C400 had a significant correlation with C470 ($R^2 > 0.9$), indicating similar characteristics and allochthonous origins. According to previous studies, C340 is a protein-like component (tryptophan-like peak T) of autochthonous origin (Coble, 1996), and C320 was similar to the protein-like (tyrosine-like peak B) component of autochthonous origin (Coble, 1996).

The biological index (BIX), a proxy for freshly produced autochthonous DOM, was calculated as the ratio of the emission intensity at 380 nm divided by that at 430 nm, with a fixed excitation wavelength of 310 nm (Huguet et al., 2009). Higher BIX values indicate a higher proportion of freshly produced DOM.

The absorption coefficient at λ nm ($a_{CDOM}(\lambda)$ in m^{-1}) was calculated by the following equation:

$$a_{CDOM}(\lambda) = 2.303A(\lambda)/l$$

where the factor 2.303 is the natural logarithm of 10, $A(\lambda)$ is the absorbance at wavelength λ in nm, and l is the optical path length in meters (Stedmon & Markager, 2001). The absorption coefficient at 350 nm ($a_{CDOM}(350)$) has been suggested as a proxy for CDOM concentration, and used to estimate the inputs of terrigenous DOM and lignin phenol concentrations in the Arctic (Fichot et al., 2016; Spencer et al., 2009; Walker et al., 2013).

The spectral slope of CDOM absorption was calculated over a range of 275–295 nm ($S_{275-295}$ in nm^{-1}; Helms et al., 2008), and over the 300–650 nm range using non-linear least squares fitting ($S_{300-650}$ in μm^{-1}; Stedmon & Markager, 2001). The spectral slope of CDOM is inversely proportional to molecular weight (Stedmon &

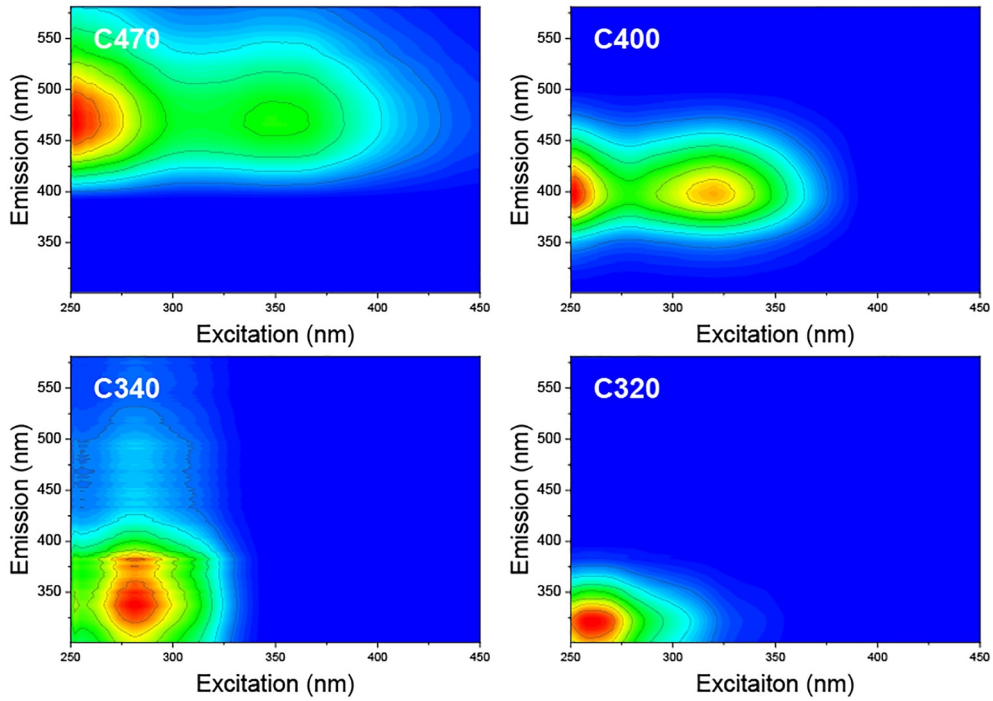

Figure 2. Contour plots of the four-component PARAFAC model developed from fluorescence excitation-emission matrices (EEMs) recorded for all DOM samples during the MOSAiC, N-ICE2015 and TA19_4 expeditions.

Nelson, 2015). $S_{300-650}$ is used to characterize DOM composition and photochemical transformation (Helms et al., 2008; Nelson & Siegel, 2013). $S_{300-650}$ and the absorption coefficient at 375 nm ($a_{CDOM}(375)$) were used to distinguish marine from terrestrial CDOM based on the model by Stedmon and Markager (2001). The specific ultraviolet absorbance ($SUVA_{254}$ in L mg^{-1} m^{-1}) was calculated by the absorbance at 254 nm (given in m^{-1}) divided by the DOC concentration in mg L^{-1} (Weishaar et al., 2003). $SUVA_{254}$ has been previously used as a proxy for aromaticity of aquatic humic substances and is positively correlated with molecular weight (Weishaar et al., 2003).

2.6. Chlorophyll-a Measurement

Chl-a samples were extracted in 90% acetone at 4°C over night, homogenized using a cell mill, and measured on the following day using a fluorometer (TD-700; Turner Designs, USA), followed by an acidification step to determine phaeopigments (see Knap et al. (1996) for details and calculations).

2.7. Statistical Analysis

The software Origin (Version 2018, OriginLab Corporation, Northampton, MA, USA) was used to conduct principal component analysis (PCA) to assess the variability of optical properties in two contexts: (a) among different water masses, and (b) within the PSW samples in different regions. The optical properties considered in the analysis included two humic-like fluorescent components (C470, C400), BIX, $a_{CDOM}(350)$, and $S_{300-650}$. Before conducting the PCA, these parameters were normalized using z-score normalization, which involves subtracting the mean and dividing by the standard deviation. In addition, a one-way ANOVA test (aov() function in R; $p < 0.01$) was conducted to assess the seasonal differences of the FDOM components and Chl-a in PSW of the Amundsen Basin during MOSAiC. Eighteen duplicate DOM samples were stored, both, at 4°C and −20°C. A non-parametric Wilcox signed-rank test (Version 2018, OriginLab Corporation, Northampton, MA, USA) was used to assess if the optical DOM parameters (C470, C400, C340, C320, BIX, $S_{275-295}$, $S_{300-650}$, $a_{CDOM}(254)$, $a_{CDOM}(350)$, $a_{CDOM}(375)$, and $a_{CDOM}(650)$; Table S2 in Supporting Information S1) were significantly different ($p < 0.01$) at different storage temperatures.

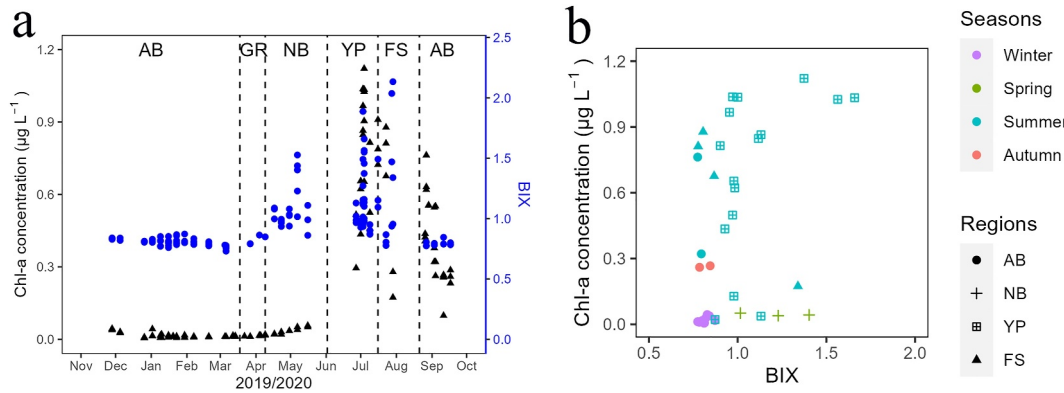

Figure 3. Polar surface water characteristics: (a) Temporal changes of chlorophyll-a concentration (Chl-a; black dots) and the biological index (BIX; blue triangle) in different regions. (b) Relationship between Chl-a and corresponding BIX in different seasons (colors) and regions (shapes). AB: Amundsen Basin, GR: Gakkel Ridge, NB: western Nansen Basin, YP: Yermak Plateau, and FS: Fram Strait. Note. Only some Chl-a samples in panel (a) are corresponding to DOM samples.

3. Results

3.1. Water Masses

The Temperature-Salinity (TS)-diagram of all marine DOM samples collected during MOSAiC revealed clear hydrographical gradients (Figure S2a in Supporting Information S1).

For PSW, S_P (Figures S2b–S2d in Supporting Information S1) ranged from 29.0 to 33.3 (with a mean ± SD of 31.8 ± 1.0) in the Amundsen Basin, from 31.1 to 32.8 (with a mean ± SD of 31.7 ± 0.4) in the Fram Strait, from 34.2 to 34.3 (with a mean ± SD of 34.3 ± 0.1) in the western Nansen Basin, and from 32.5 to 34.1 (with a mean ± SD of 33.8 ± 0.2) on the Yermak Plateau. While the surface temperature was close to the freezing point in winter (Figure S3a in Supporting Information S1, deviation of 0.003 ± 0.005°C), their deviation increased to 0.113 ± 0.003°C in mid-April, indicating the beginning of spring. The AW was primarily observed at depths ranging from 100 to 700 m. Within the AW layer (Figure S3b in Supporting Information S1), the maximum temperature was 1.57°C (with a mean ± SD of 0.82 ± 0.46°C) in the Amundsen Basin, 1.71°C (with a mean ± SD of 1.05 ± 0.50°C) in the western Nansen Basin, 2.61°C (with a mean ± SD of 1.12 ± 0.64°C) on the Yermak Plateau, and 2.66°C (with a mean ± SD of 0.97 ± 0.72°C) in the Fram Strait.

To assess the seasonal differences of the FDOM composition and Chl-a in PSW of the Amundsen Basin, a one-way ANOVA was performed using seasons as factors (Table S3 in Supporting Information S1). We found no statistically significant seasonal differences in the terrestrial FDOM components C470, and C400 ($p > 0.01$; Table S3 in Supporting Information S1). However, the analysis did show statistically significant differences between seasons for BIX and Chl-a ($p < 0.01$; Table S3 in Supporting Information S1). Relatively high concentrations of BIX, and Chl-a were observed after the spring season (Figure 3). However, there was no significant correlation between BIX and Chl-a in PSW (ANOVA, $p < 0.01$; Figure 3b).

The C340, C320, $a_{CDOM}(254)$, and $S_{275-295}$ were significantly different between the 4°C and −20°C storage (Wilcoxon rank sum test, $p < 0.01$), in contrast to C470, C400, $a_{CDOM}(350)$, $a_{CDOM}(375)$, $a_{CDOM}(650)$, BIX and $S_{300-650}$ (Wilcoxon rank sum test, $p > 0.01$). Hence, we selected BIX and $S_{300-650}$ and ignored C340, C320 and $S_{275-295}$ for the PCA. PCA was used to explore the variability of optical properties among different water masses (PSW, UHC, LHC, AW1, AW2, and DW; Figures 4a and 4b). The goal was to understand how optical properties vary across these different water masses and to identify the main sources of variability. The results of the PCA revealed that Principal Component 1 (PC1) accounted for 64.7% of the total variance in the optical properties. PC1 was characterized by large positive loadings for C470, C400, and $a_{CDOM}(350)$, indicating that these variables contributed most to the variability of water masses. The pattern suggested a relatively high contribution of terrestrial sources of CDOM. Furthermore, a significant linear relationship was observed between the DOC concentration and the PC1 score for all water masses ($R^2 = 0.81$), indicating that higher DOC levels, primarily in PSW and UHC, were associated with a terrigenous source of organic matter. Conversely, lower DOC levels, mainly in AW1, AW2 and DW, were related to a marine organic matter. Principal Component 2 (PC2) explained

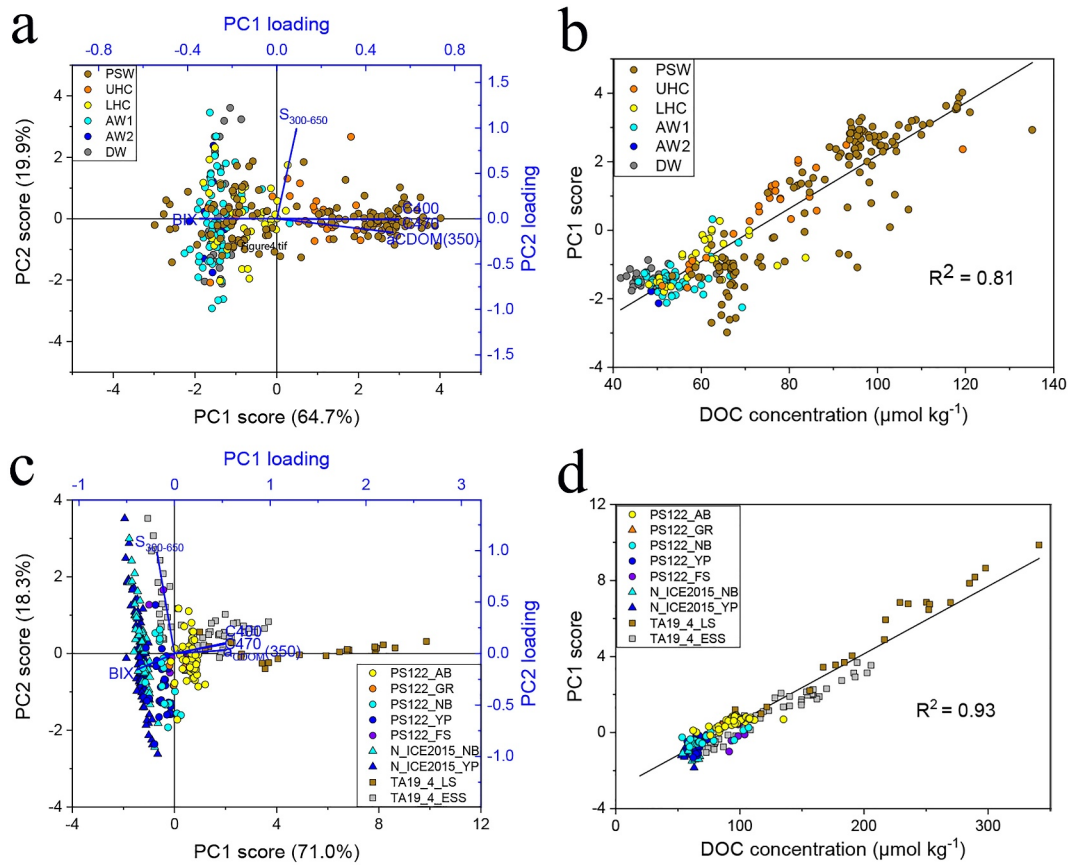

Figure 4. Optical characteristics of water masses during MOSAiC: differences in water masses as revealed by (a) principal component analysis (biplot) based on optical parameters (C470, C400, BIX, $a_{CDOM}(350)$ and $S_{300-650}$), and (b) the relationship between DOC and principal component 1 (PC1) score. Regional differences in polar surface water: (c) PCA biplot, and (d) the relationship between DOC and PC1 score during MOSAiC, N-ICE2015 and TA19_4 expeditions. Loadings for the six variables are represented in blue. PSW: Polar surface water, UHC: Upper Halocline, LHC: Lower Halocline, AW1: Upper Atlantic Water, AW2: Lower Atlantic Water, and DW: Deep Water. AB: Amundsen Basin, GR: Gakkel Ridge, NB: western Nansen Basin, YP: Yermak Plateau, FS: Fram Strait, LS: Laptev Sea, and ESS: East Siberian Sea.

19.9% of the total variance in the optical properties, and exhibited a strong positive loading for $S_{300-650}$, suggesting a contribution of photo degradation processes.

PCA was also applied to the optical properties of PSW samples to investigate their spatial variability. The goal was to identify the dominant optical properties of PSW in different regions (Figures 4c and 4d). PC1 explained 71.0% of the total variance and effectively separated PSW collected in the Laptev Sea, East Siberian Sea, and Amundsen Basin from those collected in the western Nansen Basin and Yermak Plateau. PC1 exhibited strong positive loadings for C470, C400, and $a_{CDOM}(350)$, indicating a relatively high contribution of CDOM from terrestrial sources. Samples with positive PC1 scores were primarily of terrestrial origin, and samples located at the right of the PCA biplot represented end members from Siberian shelves (Figure 4c). On the other hand, most samples from the western Nansen Basin and Yermak Plateau, with negative PC1 scores, was characterized by a lower contribution of terrestrial CDOM. A significant linear relationship was observed between the DOC concentration and the PC1 score for all water masses ($R^2 = 0.93$; Figure 4d), also suggesting a predominant terrestrial CDOM in PSW. PC2 explained 18.3% of the total variance in the optical properties, and exhibited a strong positive loading for $S_{300-650}$. This loading was related to the photochemical alterations of CDOM in PSW, particularly within the Nansen Basin, Yermak Plateau and Siberian shelves.

Based on the model developed by Stedmon and Markager (2001; SM2001) the relationship between $S_{300-650}$ and $a_{CDOM}(375)$ was utilized to distinguish marine CDOM from terrestrial CDOM. The model provides a threshold

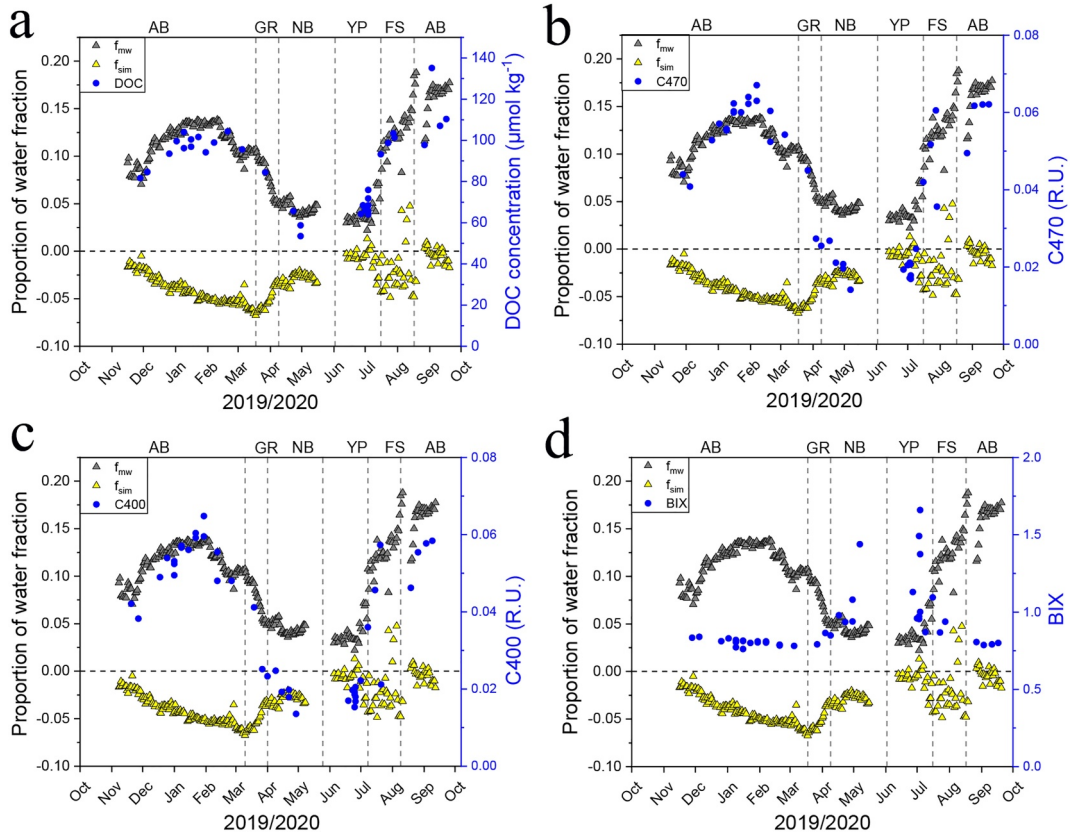

Figure 5. Polar surface water: meteoric water fraction (f_{mw}), sea ice melt water (f_{sim}) and corresponding (a) DOC concentration, and PARAFAC components (b) C470, (c) C400, and (d) biological index (BIX) in polar surface water (PSW) over the entire duration of the MOSAiC expedition. Dashed vertical lines separate different regions. Dashed horizontal line represents the zero value of the left *y*-axis. AB: Amundsen Basin, GR: Gakkel Ridge, NB: western Nansen Basin, YP: Yermak Plateau, and FS: Fram Strait.

for this discrimination (Figure S4 in Supporting Information S1). Data points that fall within the region between the dashed lines (within the model limits) are considered to represent marine CDOM, indicating that they align with the expected relationship between $S_{300-650}$ and $a_{CDOM}(375)$ for marine sources. On the other hand, data points that lie outside the model limits are classified as terrestrial CDOM, suggesting that they deviate from the expected relationship and originate from terrestrial sources. In our study, the water masses PSW and UHC were predominantly associated with terrestrial CDOM. Samples in PSW or UHC collected in the Amundsen Basin and Fram Strait exhibited larger deviations from the model limits compared to the samples from the western Nansen Basin and Yermak Plateau.

3.2. Sources of Surface Waters

To assess the contribution of meteoric water f_{mw} and sea ice melt water f_{sim} (as described by Equations 1–3) in surface waters, a three-endmember mass balance approach was used (Figure 5). The f_{mw} values ranged from 0.06 to 0.18 (with a mean ± SD of 0.12 ± 0.03) in the Amundsen Basin, from 0.04 to 0.06 (with a mean ± SD of 0.05 ± 0.01) in the western Nansen Basin, from 0.02 to 0.07 (with a mean ± SD of 0.04 ± 0.01) on the Yermak Plateau, and from 0.08 to 0.19 (with a mean ± SD of 0.13 ± 0.02) in the western Fram Strait. The Amundsen Basin and western Fram Strait had significantly higher meteoric fraction in the surface waters, which corresponded to higher concentrations of DOC, and higher levels of the FDOM humic-like components (C470, and C400) (Figures 5a–5c). In contrast, there was no clear relationship between meteoric water and autochthonous DOM, and sea ice melt and autochthonous DOM (Figure 5d).

3.3. Vertical Variations in the DOM Composition

One of the challenges of the MOSAiC expedition was to reach consistent high-quality sampling over all five consecutive teams that joined the cruise. For quality control, we evaluated the variance of the DOC concentration and PARAFAC components C470 and C400 in all deep-water samples (Figure S5 in Supporting Information S1). Due to the limited input and the predominant refractory character of DOM in the deep ocean (Hansell, 2013; Hansell et al., 2012), DOM quantity and characteristics in the deep basins remain relatively constant. The coefficient of variation in PSW was higher, with values ≥17% for DOC concentration and ≥34% for all FDOM humic-like components. For samples in deep water, we observed a coefficient of variation for the DOC concentration below 4.9%, which was similar to the analytical repeatability of the method and supported the conclusion that the teams carried out consistent sampling over the course of the cruise. As expected, the coefficient of variation in PSW was markedly higher in comparison to deep water (Figure S5 in Supporting Information S1) as a consequence of seasonal and regional differences in the surface. The TS-diagram (Figures S2b–S2d in Supporting Information S1) also showed pronounced differences in DOC concentration and humic-like components (C470 and C400) in PSW compared to AW and DW.

Expectedly, PSW exhibited lower TDN concentrations and higher DOC, $SUVA_{254}$, $a_{CDOM}(350)$, $a_{CDOM}(375)$, C470, and C400 compared to deeper waters below (Figure 6; Figures S2b–S2d and Table S4 in Supporting Information S1). When comparing only PSW, higher TDN concentrations were observed in the western Nansen Basin and Yermak Plateau compared to the Amundsen Basin and Fram Strait. BIX values were relatively high in surface waters of the western Nansen Basin, Yermak Plateau, and the Fram Strait compared to the Amundsen Basin. During a strong storm in the Amundsen Basin on 6 March 2020, we observed 27% higher DOC concentration, 41% higher $SUVA_{254}$ value, 107% higher C470 value, but 31% lower TDN concentration, and 23% lower BIX at ∼200 m water depth compared to samples collected at the same depth in January and February.

During the drift of ice-tethered buoy ITP94 across the Amundsen Basin from October 2019 to March 2020, DOM fluorescence in PSW increased over time (Figure 7b, see also and Figure S6b in Supporting Information S1). The highest values were observed between January and March. FDOM values for $S_P \sim 32.5$ ranged from 0.015 to 0.042 R.U. in the Amundsen Basin (Figure 7a), for example, The maximum temperatures were observed in the AW layer over the Yermak Plateau and Fram Strait (Figure S6a in Supporting Information S1), consistent with observations from CTD rosette data during MOSAiC.

3.4. Lead Waters

The analysis of low-salinity ($2.4 \leq S_p \leq 20$) surface water samples collected in open water leads in the Amundsen Basin in late summer revealed a significant positive linear correlation between S_p and DOC ($R^2 = 0.89$; Figure 8a). Similarly, there was a significant positive correlation between S_p and the FDOM components C470, and C400 (R^2 of 0.90 and 0.88, respectively; not shown). In a PCA analysis, PC1 accounted for 80.0% of the total variance and effectively differentiated between high-salinity ($28 \leq S_p \leq 30$) and low-salinity lead water samples (Figure 8b). In high-salinity lead water samples, PC1 was dominated by terrestrial CDOM, indicated by strong positive loadings for C470, C400 and $a_{CDOM}(350)$. Conversely, low-salinity lead water samples were characterized by autochthonous CDOM, as indicated by strong negative loadings for the optical parameters BIX and $S_{300-650}$ in PC1. PC2 accounted for 17.0% of the total variance in the optical properties, displaying a notable positive loading for BIX, suggesting the influence of local production of CDOM for low-salinity lead water samples. Additionally, it exhibited a negative loading for $S_{300-650}$, indicative of photochemical degradation of CDOM for low-salinity lead water samples.

4. Discussion

4.1. Regional Variations of DOM Characteristics

Polar surface water showed distinct regional differences in optical characteristics in the Eurasian Basin, which can be mainly attributed to the varying contribution of terrestrial organic matter transported via the TPD. Multivariate statistics (PCA) could explain a high proportion of the variance in the optical parameters by principal component 1 (PC1) that was constituted by those optical parameters that gave a good representation of the terrestrial contribution in PSW and UHC water in different regions (East Siberian Sea, Laptev Sea and Amundsen Basin). Consequently, we observed a significant correlation between DOC concentration and the PC1 score (Figure 4).

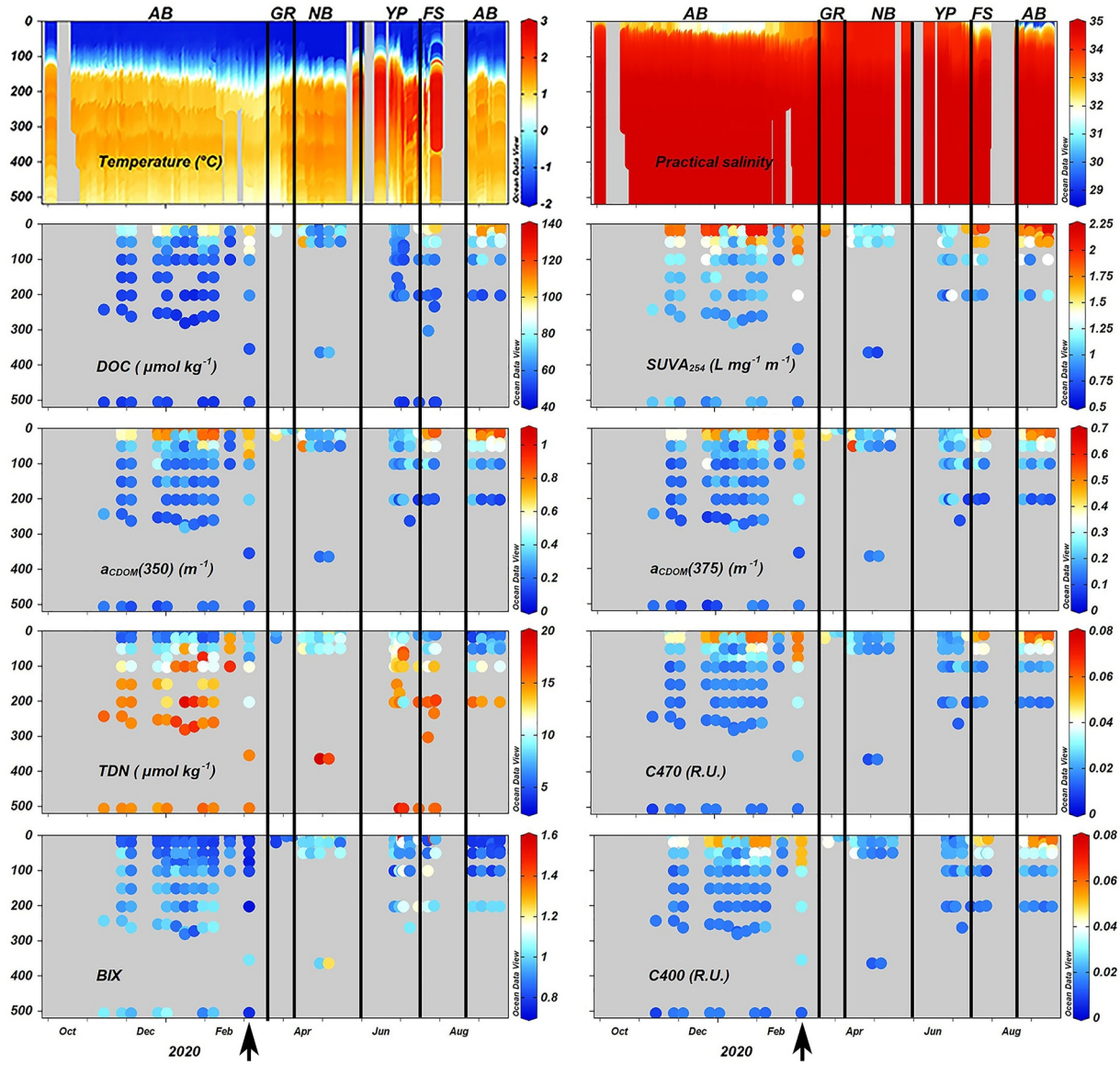

Figure 6. Upper ocean vertical profiles of temperature, practical salinity, DOC concentration, $SUVA_{254}$, $a_{CDOM}(350)$, $a_{CDOM}(375)$, total dissolved nitrogen (TDN) concentration, C470, biological index (BIX), and C400 (arranged from upper left to lower right) in the upper 500 m over the entire duration of MOSAiC. Black arrows: storm event. Solid vertical black lines separate different regions. AB: Amundsen Basin, GR: Gakkel Ridge, NB: western Nansen Basin, YP: Yermak Plateau, and FS: Fram Strait.

Higher DOC concentrations (Table S4 in Supporting Information S1) predominantly reflected the advection of terrigenous organic matter, rather than local production and degradation processes (Mann et al., 2016; Opsahl et al., 1999). The SM2001 model (Figure S4a in Supporting Information S1) confirmed the association between CDOM characteristics and different water masses. PSW and UHC water were associated with terrestrial sources, while AW1, AW2, and DW were primarily characterized by a higher contribution of CDOM from marine-derived sources. Furthermore, $SUVA_{254}$ values were much higher in the Amundsen Basin and western Fram Strait compared to the western Nansen Basin and Yermak Plateau area (Figure 6) suggesting a dominance of humic-like substances with higher molecular weight from allochthonous input (Walker et al., 2013; Weishaar et al., 2003). DOC concentration and humic-like fluorescence components were closely associated with meteoric fraction (i.e., riverine runoff and net precipitation) (Figure 5), emphasizing that freshwater is primarily provided by Siberian rivers and net precipitation over land and transported by the TPD across the Central Arctic Ocean toward the western Fram Strait (Charette et al., 2020). The TPD affects the upper water column of most of the Amundsen and

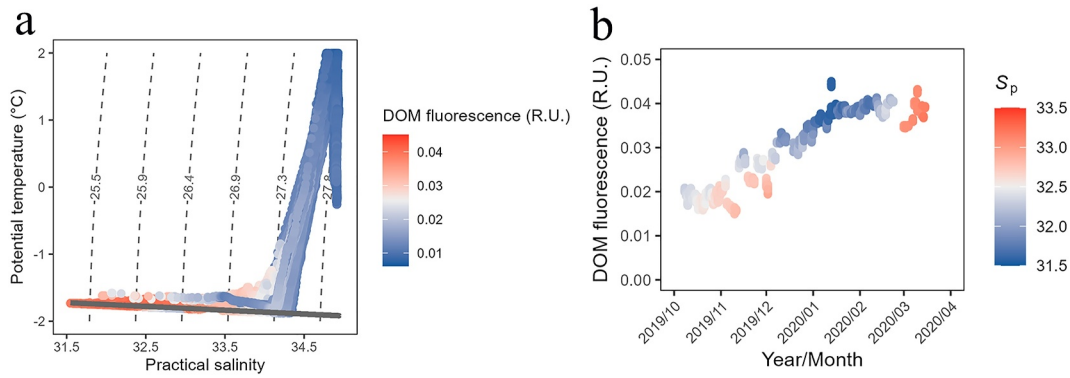

Figure 7. Temporal changes of dissolved organic matter (DOM) fluorescence in the Amundsen Basin as recorded by the ice-tethered profiling system ITP94. (a) TS-diagram (potential temperature (θ), practical salinity S_p; colors indicate DOM fluorescence). (b) Temporal evolution of DOM fluorescence for polar surface water (colors indicate practical salinity). Gray solid line: freezing point. Gray dashed lines: isopycnals.

Makarov Basins, which are separated by the Lomonosov Ridge (Slagter et al., 2017). The high proportions of meteoric water in the western part of the Fram Strait (July/August 2020; Figure 5) were derived from relatively fresh and cold PSW in the East Greenland Current (Pavlov et al., 2015). Our observations are in good agreement with previous studies reporting that terrestrial DOM from the Siberian shelves contributes significantly to the DOM composition in PSW in the Amundsen Basin (Amon et al., 2003; Boles et al., 2020; Charette et al., 2020; Slagter et al., 2017).

Continuous profiling data in the Amundsen Basin, at the start of the ITP94 drift (8 October 2019), showed that DOM fluorescence was relatively low (0.020 ± 0.0003 R.U.), while S_p was relatively high (32.3 ± 0.01; Figure 7b) in the PSW. In comparison, when examining PSW in a similar area for ITP60 in December of 2012 (data not shown), S_p was 7.5% higher and DOM fluorescence was 67.8% lower, reflecting the high interannual variability of the TPD (Krumpen et al., 2019). In March 2020, sampling locations were close to Gakkel Ridge where the influence of the Transpolar Drift was smaller, as indicated by high S_p (Figure 7b). DOM fluorescence in PSW also increased continuously from the beginning of the ITP94 drift in the Amundsen Basin until March 2020 (Figure 7b). This increase can either be attributed to the seasonal variability of riverine input or to ITP94 gradually approaching the core of the TPD (Schulz et al., 2023). Therefore, the influence of terrestrial DOM on the PSW characteristics and composition can vary within a region, depending on the specific pathway and strength of the TPD during a given period and with consequences for the regional microbial ecology. It has been shown that the

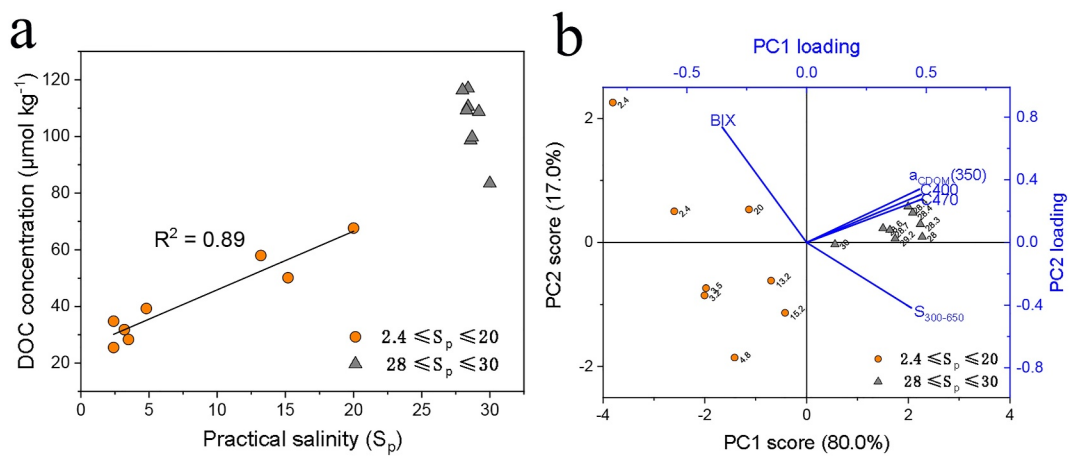

Figure 8. Dissolved organic matter characteristics in the topmost water layer of sea-ice leads in the Amundsen Basin separated into low-salinity ($2.4 \leq S_p \leq 20$; orange dots) and high-salinity ($28 \leq S_p \leq 30$; dark gray triangles) samples. (a) Relationship between DOC concentration and practical salinity (S_P) and (b) PCA biplot based on optical parameters C470, C400, biological index (BIX), absorbance ($a_{CDOM}(350)$) and spectral slope ($S_{300-650}$). Values in black indicate S_p.

location and strength of the TPD can vary considerably between years as a response to the Arctic Oscillation and seasonal variability of riverine input (Karcher et al., 2012; Mysak, 2001; Smith et al., 2021).

In contrast, the optical properties of CDOM observed in the western Nansen Basin and Yermak Plateau suggest an autochthonous origin, likely produced during phytoplankton blooms, with minimal influence from terrestrial CDOM originating from continental runoff. The Fram Strait serves as an important pathway for the inflow of warm AW from the Atlantic Ocean into the Arctic Ocean (Rudels et al., 2004). The temperature maximum within the AW layer is warmest in Fram Strait, and across Yermak Plateau and decreases further downstream before reaching the western Nansen Basin and Amundsen Basin. PSW formation in the western Nansen Basin and around the Yermak Plateau involves the entrainment and transformation of cooled AW into the surface layer during sea-ice formation and winter convection (Rudels, 1989). This is in agreement with previous studies that demonstrate that surface waters in the western Nansen Basin and Yermak Plateau were generally affected by the inflow of relatively warm, salty and nutrient-rich AW water (Pavlov et al., 2017; Rudels et al., 2015).

4.2. Temporal Changes in DOM: Sea-Ice Melt, Primary Production, and Storms

The MOSAiC expedition provided a unique opportunity to study DOM sources and characteristics in the Arctic Ocean over the course of a full year. Our initial main goal during MOSAiC was to track seasonal DOM changes in the surface ocean. Seasonal variations play a vital role in shaping the physical, biological, and biogeochemical characteristics of the Arctic Ocean. Although the variability of DOC and humic-like FDOM over all observations was highest in the upper 200 m (Figure 6 and Figure S5 in Supporting Information S1), the changes could be primarily related to varying terrestrial contributions (see above). For the MOSAiC expedition, it was challenging to unravel seasonal CDOM changes because seasonal and regional changes were superimposed. The limited temporal coverage of DOM sampling in different regions makes it difficult to assess the overall seasonal variations in DOM properties during the year-round expedition. Due to a slightly higher temporal sample resolution, we focused here on a seasonal comparison in DOM properties exclusively in the Amundsen Basin.

An ANOVA analysis (Table S3 in Supporting Information S1) provided valuable insights into the influence of seasons on the DOM composition in PSW of the Amundsen Basin, suggesting that the composition of terrestrial FDOM components ($p > 0.01$) had minimal seasonal variation. This implies that the input and characteristics of terrestrial DOM, originating from continental runoff, remain relatively constant and aged across seasons within this region. Additionally, autochthonous DOM shows less association with meteoric sources (Figures 5e and 5f). Cooper et al. (2005) suggested that ~30% of the runoff DOC is initially removed over the shelves before entering the Arctic Ocean. Kaiser et al. (2017) showed that ~50% of the annual discharge of terrestrial DOC from Siberian rivers is mineralized on the Eurasian shelves. Consequently, the most labile DOM may undergo removal on the Eurasian shelves before reaching the Central Arctic Ocean, and terrestrial DOM transported by the TPD exhibits relatively refractory characteristics.

Seasonal variations significantly influenced the composition of Chl-a and autochthonous DOM ($p < 0.01$; Table S3 in Supporting Information S1). This implies that changes in biological activity and other environmental factors associated with seasonal transitions can affect the production and characteristics of autochthonous DOM in this region. However, it is worth noting that there is little association between Chl-a and autochthonous DOM in PSW, even though the highest concentrations of autochthonous DOM and Chl-a were observed in the summer season (Figure 3). In winter, constantly low concentrations of autochthonous DOM and Chl-a were observed. Chl-a concentration is commonly used as a proxy for estimating phytoplankton biomass (Sauzède et al., 2015), which leads to the release of labile organic matter into the water column (Carlson et al., 1998; Lancelot, 1979). The primary production in the Arctic Ocean is affected by a complex interaction between different abiotic and biotic drivers, with light and nutrient availability being most important (Popova et al., 2012). Light availability in the Arctic Ocean is strongly influenced by the presence of sea ice and the properties of the sea ice, such as surface albedo (reflectivity), snow depth, and ice thickness, play a crucial role in determining how much solar radiation can penetrate into the ocean (Castellani et al., 2022). During winter, light availability is constrained by the polar night and ice cover, which resulted in a constantly low chlorophyll-a concentration. The Amundsen Basin exhibited the highest average values of $a_{CDOM}(350)$ (Figure 6 and Table S4 in Supporting Information S1) among all regions during MOSAiC and with its light-absorbing properties it can also attenuate light penetration into the water column, with implications for primary producers (Granskog et al., 2007; Lund-Hansen et al., 2015). Nutrient availability is not only affected by horizontal advection of nutrient-rich waters, in the Eurasian Basin

most prominently via the Atlantic inflow, but also by supply from upwelling (Carmack et al., 2006, 2016). The transport of high loads of riverine freshwater by the TPD result in low salinity surface waters and strong stratification, which can affect nutrient mixing and availability in the upper ocean layers (Nummelin et al., 2016). The interplay between these factors and their seasonal variations can lead to changes in primary production, with subsequent influence on the release of labile organic matter into the water column. In addition, freshly generated autochthonous DOM in the ocean can also originate from cell lysis and release by zooplankton grazing (McKnight et al., 2001; Nagata et al., 2000). Most of this newly produced DOM is biologically labile and consumed and respired rapidly by heterotrophic bacteria (Hansell et al., 2009). However, a small fraction of this autochthonous DOM escapes rapid remineralization and is transformed into refractory material by abiotic and biotic processes and accumulates in the surface layer for eventual export to the deep ocean by bottom water formation (Hansell et al., 2009). In winter, low temperatures decrease bacterial activity, thereby reducing DOM biodegradation (Sherr & Sherr, 2003), which may be related to the constant autochthonous DOM. The manifold controls on DOM production and decomposition as well as temporal decoupling from production were likely reasons for our observation that Chl-a and autochthonous DOM concentrations were decoupled, which is in agreement with previous studies (Cao et al., 2020; Carr et al., 2019; Jeon et al., 2023; Painter et al., 2018).

Few samples during MOSAiC were obtained from the uppermost surface water during the summer season in the Amundsen Basin. The analytical results of the low-salinity lead water samples demonstrated the contribution of DOM derived by sea ice melt to the autochthonous DOM fraction in the surface water (Figure 8b). For low-salinity lead water samples, we also observed a significant positive correlation between DOC concentration and salinity (Figure 8a). This was in contrast to the general observation that fluorescence and DOC concentration in PSW were mainly derived by terrestrial sources and therefore correlated negatively with salinity. This implies that freshwater input from sea ice melt plays a role in reducing salinity and diluting terrestrial DOM within surface waters. During the summer season, the impact of warming becomes more pronounced (Figure S3a in Supporting Information S1) and due to increased solar radiation and resulting sea ice melt, surface water is warming and freshening, leading to enhanced stratification. This finding aligns with previous studies suggesting the release of labile DOM by sea ice melt (Brogi et al., 2018; Zabłocka et al., 2020), with fundamental consequences for the microbial ecology in surface water (Underwood et al., 2019), and the influence of melting sea ice on the dilution of the surface water (Logvinova et al., 2016). Consequently, the interplay between DOM release from sea-ice production and its subsequent microbial turnover could also contribute to the decoupling observed between autochthonous DOM and Chl-a. Nevertheless, this decoupling may not be the sole factor governing the distribution of autochthonous DOM. Another plausible explanation for this decoupling is that the sea-ice drift speed differs from the speed of the underlying water.

Storms in winter also affect the chemical signatures at the ice water interface (Rabe et al., 2022). During MOSAiC, in the Amundsen Basin on 6 March 2020 (Figure 6), we observed major changes down to ∼200 m water depth, as indicated by higher values of DOC and optical parameters that represented terrestrial CDOM contribution, but lower TDN concentrations and biological contribution BIX. We assume that this abrupt change was related to a strong storm that occurred right before the time of sampling and that led to the deepening of the mixed layer. Consequently, the influence of the storms could shape the vertical distribution of DOM and related microbial processes in the subsurface. A previous study also reported that the transfer between AW and PSW can be affected by the vertical velocity shear below PSW, which is strengthened by strong storms in winter (Polyakov et al., 2013).

4.3. Perspective

The optical parameters and components derived from Parallel Factor Analysis were suitable to characterize water masses and FDOM sources and distribution in the surface of the Eurasian Arctic Ocean. PARAFAC components represent independent fluorophores or groups sharing very similar spectra. C470, for example, can be characterized as a mixture that was associated with aromatic, high molecular weight organic matter exhibiting terrestrial characteristics that have been shown to correlate with lignin phenol concentrations (Amon et al., 2003; Gonçalves-Araujo et al., 2016; Murphy et al., 2011). However, the exact chemical origin of these components remains unknown. Converting fluorescence intensities to concentrations is also challenging due to varying efficiencies of different fluorophores in absorbing and converting incident radiation to fluorescence (Murphy et al., 2013). Another limitation was apparent, when we performed a PCA analysis and combined lead and ocean water samples (similar to Figure 4, data not shown): the optical characteristics of lead water were indistinguishable from PSW. Additionally, all lead waters are located in the Amundsen Basin, highly influenced by TPD,

characterized by a significant contribution of terrestrial DOM. This factor may also explain the indistinguishability of PSW between lead and ocean waters based on only optical parameters. Therefore, we will carry out a follow-up study that uses Fourier Transform Ion Cyclotron Resonance Mass Spectrometry (FT-ICR MS) hyphenated with liquid chromatography to achieve additional chemical information that allows distinguishing the chemical characteristics and the quantity of DOM sources in the Central Arctic Ocean during MOSAiC. Improving our capabilities in quantifying the sources and fluxes of DOM is crucial to assess its role in the carbon cycle and how this role changes with the drastically increasing temperatures in the Arctic Ocean.

Conflict of Interest

The authors declare no conflicts of interest relevant to this study.

Data Availability Statement

CDOM absorbance data for N-ICE2015 expedition is available through the Norwegian Polar Data Centre at https://doi.org/10.21334/npolar.2017.f46970ba (Pavlov, Kauko, et al., 2016). CDOM absorbance data for TA19-4 expedition is available through the PANGAEA data repository at https://doi.org/10.1594/PANGAEA.924211 (Hölemann et al., 2020). All CDOM and DOC data for MOSAiC, as well as EEMs data for MOSAiC, N-ICE2015 and TA19-4 expeditions are archived in the PANGAEA data repository at https://doi.org/10.1594/PANGAEA.948019 (Kong et al., 2022). CTD profile data on the Central Observatory ice floe (Ocean City; https://doi.org/10.1594/PANGAEA.959964; Tippenhauer et al., 2023a) and on RV Polarstern (https://doi.org/10.1594/PANGAEA.959963; Tippenhauer et al., 2023b) during the MOSAiC expedition are available from the PANGAEA data repository. CTD bottle data for DOM samples on the Ocean City; (https://doi.org/10.1594/PANGAEA.959966; Tippenhauer et al., 2023c) and on RV Polarstern (https://doi.org/10.1594/PANGAEA.959965; Tippenhauer et al., 2023d) are available from the PANGAEA data repository. The stable oxygen isotope ratio ($\delta^{18}O$) and corresponding practical salinity are available from the PANGAEA data repository at https://doi.org/10.1594/PANGAEA.948291 (Mellat et al., 2022). Chl-a concentrations from CTD casts during the MOSAiC expedition are available from the PANGAEA data repository at https://doi.pangaea.de/10.1594/PANGAEA.963277 (Hoppe et al., 2023). The Ice-Tethered Profiler data is collected by the Ice-Tethered Profiler Program (Krishfield et al., 2008; Toole et al., 2011) based at the Woods Hole Oceanographic Institution (https://www2.whoi.edu/site/itp/). Some figures are illustrated using Ocean Data View software (Schlitzer, Reiner, Ocean Data View, https://odv.awi.de, 2023).

Acknowledgments

This work was carried out, and data used in this manuscript were produced, as part of the international Multi-disciplinary drifting Observatory for the Study of Arctic Climate (MOSAiC) with the tag MOSAiC20192020. We thank all persons involved in the expedition of the Research Vessel Polarstern during MOSAiC in 2019–2020 (AWI_PS122_00) as listed in Nixdorf et al. (2021). MAG was supported by the Research Council of Norway (Grant 280292). MV was funded by the Changing Arctic Ocean (CAO) program, jointly funded by the United Kingdom Research and Innovation (UKRI), Natural Environment Research Council (NERC) and the Bundesministerium für Bildung und Forschung (BMBF), project Advective Pathways of nutrients and key Ecological substances in the ARctic (APEAR) Grants NE/R012865/1, NE/R012865/2, and 03V01461. The authors are thankful to Claudia Burau for supporting the DOC analyses, Jens A. Hölemann for providing CDOM data for TA19_4 expedition, Benjamin Rabe for providing CTD data for MOSAiC expedition, and John Paul Balmonte, Jeff Bowman, Emelia Chamberlain, Jessie M. Creamean, Elise Droste, Lena Eggers, Oliver Müller, Lasse Mork Olsen, Sinhué Torres-Valdes and Laura Wischnewski for collecting Chl-a or CDOM and DOC samples during the MOSAiC expedition. Open Access funding enabled and organized by Projekt DEAL.

References

Amon, R. M. W., Budéus, G., & Meon, B. (2003). Dissolved organic carbon distribution and origin in the Nordic Seas: Exchanges with the Arctic Ocean and the North Atlantic. *Journal of Geophysical Research*, *108*(C7), 3221. https://doi.org/10.1029/2002JC001594

Baker, A., & Spencer, R. G. M. (2004). Characterization of dissolved organic matter from source to sea using fluorescence and absorbance spectroscopy. *The Science of the Total Environment*, *333*(1–3), 217–232. https://doi.org/10.1016/j.scitotenv.2004.04.013

Bauch, D., Dmitrenko, I. A., Wegner, C., Hölemann, J., Kirillov, S. A., Timokhov, L. A., & Kassens, H. (2009). Exchange of Laptev Sea and Arctic Ocean halocline waters in response to atmospheric forcing. *Journal of Geophysical Research*, *114*(C5), C05008. https://doi.org/10.1029/2008JC005062

Bélanger, S., Xie, H., Krotkov, N., Larouche, P., Vincent, W. F., & Babin, M. (2006). Photomineralization of terrigenous dissolved organic matter in Arctic coastal waters from 1979 to 2003: Interannual variability and implications of climate change. *Global Biogeochemical Cycles*, *20*(4), GB4005. https://doi.org/10.1029/2006GB002708

Boles, E., Provost, C., Garçon, V., Bertosio, C., Athanase, M., Koenig, Z., & Sennéchael, N. (2020). Under-ice phytoplankton blooms in the central Arctic Ocean: Insights from the first biogeochemical IAOOS platform drift in 2017. *Journal of Geophysical Research: Oceans*, *125*(3), e2019JC015608. https://doi.org/10.1029/2019JC015608

Brogi, S. R., Derrien, M., & Hur, J. (2019). In-Depth assessment of the effect of sodium azide on the optical properties of dissolved organic matter. *Journal of Fluorescence*, *29*(4), 877–885. https://doi.org/10.1007/s10895-019-02398-w

Brogi, S. R., Ha, S.-Y., Kim, K., Derrien, M., Lee, Y. K., & Hur, J. (2018). Optical and molecular characterization of dissolved organic matter (DOM) in the Arctic ice core and the underlying seawater (Cambridge Bay, Canada): Implication for increased autochthonous DOM during ice melting. *The Science of the Total Environment*, *627*, 802–811. https://doi.org/10.1016/j.scitotenv.2018.01.251

Cao, F., Zhu, Y., Kieber, D. J., & Miller, W. L. (2020). Distribution and photo-reactivity of chromophoric and fluorescent dissolved organic matter in the Northeastern North Pacific Ocean. *Deep Sea Research Part I: Oceanographic Research Papers*, *155*, 103168. https://doi.org/10.1016/j.dsr.2019.103168

Carlson, C. A., Ducklow, H. W., Hansell, D. A., & Smith Jr, W. O. (1998). Organic carbon partitioning during spring phytoplankton blooms in the Ross Sea polynya and the Sargasso Sea. *Limnology & Oceanography*, *43*(3), 375–386. https://doi.org/10.4319/lo.1998.43.3.0375

Carlson, C. A., & Hansell, D. A. (2015). DOM sources, sinks, reactivity, and budgets. In D. A. Hansell, & C. A. Carlson (Eds.), *C. A. B. T.-B. of M. D. O. M.*, *Biogeochemistry of marine dissolved organic matter* (pp. 65–126). Elsevier. https://doi.org/10.1016/B978-0-12-405940-5.00003-0

Carmack, E., Barber, D., Christensen, J., Macdonald, R., Rudels, B., & Sakshaug, E. (2006). Climate variability and physical forcing of the food webs and the carbon budget on panarctic shelves. *Progress in Oceanography*, *71*(2–4), 145–181. https://doi.org/10.1016/j.pocean.2006.10.005

Carmack, E. C., Yamamoto-Kawai, M., Haine, T. W. N., Bacon, S., Bluhm, B. A., Lique, C., et al. (2016). Freshwater and its role in the Arctic Marine System: Sources, disposition, storage, export, and physical and biogeochemical consequences in the Arctic and global oceans. *Journal of Geophysical Research: Biogeosciences*, *121*(3), 675–717. https://doi.org/10.1002/2015JG003140

Carr, N., Davis, C. E., Blackbird, S., Daniels, L. R., Preece, C., Woodward, M., & Mahaffey, C. (2019). Seasonal and spatial variability in the optical characteristics of DOM in a temperate shelf sea. *Progress in Oceanography*, *177*, 101929. https://doi.org/10.1016/j.pocean.2018.02.025

Castellani, G., Veyssière, G., Karcher, M., Stroeve, J., Banas, S. N., Bouman, A. H., et al. (2022). Shine a light: Under-ice light and its ecological implications in a changing Arctic Ocean. *Ambio*, *51*(2), 307–317. https://doi.org/10.1007/s13280-021-01662-3

Charette, M. A., Kipp, L. E., Jensen, L. T., Dabrowski, J. S., Whitmore, L. M., Fitzsimmons, J. N., et al. (2020). The transpolar drift as a source of riverine and shelf-derived trace elements to the Central Arctic Ocean. *Journal of Geophysical Research: Oceans*, *125*(5), e2019JC015920. https://doi.org/10.1029/2019JC015920

Coble, P. G. (1996). Characterization of marine and terrestrial DOM in seawater using excitation-emission matrix spectroscopy. *Marine Chemistry*, *51*(4), 325–346. https://doi.org/10.1016/0304-4203(95)00062-3

Cooper, L. W., Benner, R., McClelland, J. W., Peterson, B. J., Holmes, R. M., Raymond, P. A., et al. (2005). Linkages among runoff, dissolved organic carbon, and the stable oxygen isotope composition of seawater and other water mass indicators in the Arctic Ocean. *Journal of Geophysical Research*, *110*(G2), G02013. https://doi.org/10.1029/2005JG000031

Fichot, C. G., Benner, R., Kaiser, K., Shen, Y., Amon, R. M. W., Ogawa, H., & Lu, C.-J. (2016). Predicting dissolved lignin phenol concentrations in the coastal ocean from chromophoric dissolved organic matter (CDOM) absorption coefficients. *Frontiers in Marine Science*, *3*, 7. https://doi.org/10.3389/fmars.2016.00007

Frey, K. E., & Smith, L. C. (2005). Amplified carbon release from vast West Siberian peatlands by 2100. *Geophysical Research Letters*, *32*(9), L09401. https://doi.org/10.1029/2004GL022025

Friedlingstein, P., O'Sullivan, M., Jones, M. W., Andrew, R. M., Gregor, L., Hauck, J., et al. (2022). Global carbon budget 2022. *Earth System Science Data*, *14*(11), 4811–4900. https://doi.org/10.5194/essd-14-4811-2022

Gonçalves-Araujo, R., Granskog, M. A., Bracher, A., Azetsu-Scott, K., Dodd, P. A., & Stedmon, C. A. (2016). Using fluorescent dissolved organic matter to trace and distinguish the origin of Arctic surface waters. *Scientific Reports*, *6*(1), 33978. https://doi.org/10.1038/srep33978

Gonçalves-Araujo, R., Rabe, B., Peeken, I., & Bracher, A. (2018). High colored dissolved organic matter (CDOM) absorption in surface waters of the central-eastern Arctic Ocean: Implications for biogeochemistry and ocean color algorithms. *PLoS One*, *13*(1), e0190838. https://doi.org/10.1371/journal.pone.0190838

Granskog, M. A., Fer, I., Rinke, A., & Steen, H. (2018). Atmosphere-ice-ocean-ecosystem processes in a thinner Arctic sea ice regime: The Norwegian young sea ICE (N-ICE2015) expedition. *Journal of Geophysical Research: Oceans*, *123*(3), 1586–1594. https://doi.org/10.1002/2017JC013328

Granskog, M. A., Macdonald, R. W., Mundy, C.-J., & Barber, D. G. (2007). Distribution, characteristics and potential impacts of chromophoric dissolved organic matter (CDOM) in Hudson Strait and Hudson Bay, Canada. *Continental Shelf Research*, *27*(15), 2032–2050. https://doi.org/10.1016/j.csr.2007.05.001

Granskog, M. A., Stedmon, C. A., Dodd, P. A., Amon, R. M. W., Pavlov, A. K., De Steur, L., & Hansen, E. (2012). Characteristics of colored dissolved organic matter (CDOM) in the Arctic outflow in the Fram Strait: Assessing the changes and fate of terrigenous CDOM in the Arctic Ocean. *Journal of Geophysical Research*, *117*(C12), C12021. https://doi.org/10.1029/2012JC008075

Guéguen, C., Itoh, M., Kikuchi, T., Eert, J., & Williams, W. J. (2015). Variability in dissolved organic matter optical properties in surface waters in the Amerasian Basin. *Frontiers in Marine Science*, *2*, 78. https://doi.org/10.3389/fmars.2015.00078

Hach, P. F., Marchant, H. K., Krupke, A., Riedel, T., Meier, D. V., Lavik, G., et al. (2020). Rapid microbial diversification of dissolved organic matter in oceanic surface waters leads to carbon sequestration. *Scientific Reports*, *10*(1), 13025. https://doi.org/10.1038/s41598-020-69930-y

Hansell, D. A. (2013). Recalcitrant dissolved organic carbon fractions. *Annual Review of Marine Science*, *5*(1), 421–445. https://doi.org/10.1146/annurev-marine-120710-100757

Hansell, D. A., & Carlson, C. A. (2001). Biogeochemistry of total organic carbon and nitrogen in the Sargasso Sea: Control by convective overturn. *Deep Sea Research Part II: Topical Studies in Oceanography*, *48*(8–9), 1649–1667. https://doi.org/10.1016/S0967-0645(00)00153-3

Hansell, D. A., Carlson, C. A., Repeta, D. J., & Schlitzer, R. (2009). Dissolved organic matter in the Ocean: A controversy stimulates new insights. *Oceanography*, *22*(4), 202–211. https://doi.org/10.5670/oceanog.2009.109

Hansell, D. A., Carlson, C. A., & Schlitzer, R. (2012). Net removal of major marine dissolved organic carbon fractions in the subsurface ocean. *Global Biogeochemical Cycles*, *26*(1). https://doi.org/10.1029/2011GB004069

Helms, J. R., Stubbins, A., Ritchie, J. D., Minor, E. C., Kieber, D. J., & Mopper, K. (2008). Absorption spectral slopes and slope ratios as indicators of molecular weight, source, and photobleaching of chromophoric dissolved organic matter. *Limnology & Oceanography*, *53*(3), 955–969. https://doi.org/10.4319/lo.2008.53.3.0955

Hill, V. J. (2008). Impacts of chromophoric dissolved organic material on surface ocean heating in the Chukchi Sea. *Journal of Geophysical Research*, *113*(C7), C07024. https://doi.org/10.1029/2007JC004119

Hirose, K. (2007). Metal–organic matter interaction: Ecological roles of ligands in oceanic DOM. *Applied Geochemistry*, *22*(8), 1636–1645. https://doi.org/10.1016/j.apgeochem.2007.03.042

Hölemann, J. A., Chetverova, A., Juhls, B., & Kusse-Tiuz, N. (2020). Colored dissolved organic matter (CDOM) and dissolved organic carbon (DOC) measured during cruise TRANSARKTIKA-2019 Leg4, Laptev Sea and East Siberian Sea [Dataset]. *PANGAEA*. https://doi.org/10.1594/PANGAEA.924211

Hölemann, J. A., Juhls, B., Bauch, D., Janout, M., Koch, B. P., & Heim, B. (2021). The impact of the freeze–melt cycle of land-fast ice on the distribution of dissolved organic matter in the Laptev and East Siberian seas (Siberian Arctic). *Biogeosciences*, *18*(12), 3637–3655. https://doi.org/10.5194/bg-18-3637-2021

Hoppe, C. J. M., Heitmann, L., Brenneis, T., Terbrüggen, A., Vortkamp, M., Chamberlain, E., et al. (2023). Water column Chlorophyll a concentrations during the MOSAiC expedition (PS122) in the Central Arctic Ocean 2019-2020 [Dataset]. *PANGAEA*. https://doi.org/10.1594/PANGAEA.963277

Huguet, A., Vacher, L., Relexans, S., Saubusse, S., Froidefond, J. M., & Parlanti, E. (2009). Properties of fluorescent dissolved organic matter in the Gironde Estuary. *Organic Geochemistry*, *40*(6), 706–719. https://doi.org/10.1016/j.orggeochem.2009.03.002

Jeon, M. H., Jung, J., Park, M. O., Cho, K.-H., Lee, Y., Yang, E. J., & Kang, S.-H. (2023). Characterization and source of fluorescent dissolved organic matter in the Western Arctic Ocean: New insights from the 2019 summer study. *Frontiers in Marine Science*, *10*, 1199893. https://doi.org/10.3389/fmars.2023.1199893

Jones, E. P., Anderson, L. G., Jutterström, S., Mintrop, L., & Swift, J. H. (2008). Pacific freshwater, river water and sea ice meltwater across Arctic Ocean basins: Results from the 2005 Beringia Expedition. *Journal of Geophysical Research*, *113*(C8), C08012. https://doi.org/10.1029/2007JC004124

Kaiser, K., Benner, R., & Amon, R. M. W. (2017). The fate of terrigenous dissolved organic carbon on the Eurasian shelves and export to the North Atlantic. *Journal of Geophysical Research: Oceans*, *122*(1), 4–22. https://doi.org/10.1002/2016JC012380

Karcher, M., Smith, J. N., Kauker, F., Gerdes, R., & Smethie Jr, W. M. (2012). Recent changes in Arctic Ocean circulation revealed by iodine-129 observations and modeling. *Journal of Geophysical Research*, *117*(C8), C08007. https://doi.org/10.1029/2011JC007513

Knap, A. H., Michaels, A., Close, A., Ducklow, H., & Dickson, A. (1996). *Protocols for the joint global ocean flux study (JGOFS) core measurements*. JGOFS, Reprint of the IOC Manuals and Guides No. 29, UNESCO 1994.

Knust, R. (2017). Polar research and supply vessel POLARSTERN operated by the Alfred-Wegener-Institute. *Journal of Large-Scale Research Facilities JLSRF*, *3*, A119. https://doi.org/10.17815/jlsrf-3-163

Kong, X., Granskog, M. A., Hoppe, C. J. M., Fong, A. A., Stedmon, C. A., Tippenhauer, S., et al. (2022). *The composition of chromophoric dissolved organic matter in Central Arctic surface waters during the MOSAiC expedition*. PANGAEA. https://doi.org/10.1594/PANGAEA.948019

Korhonen, M., Rudels, B., Marnela, M., Wisotzki, A., & Zhao, J. (2013). Time and space variability of freshwater content, heat content and seasonal ice melt in the Arctic Ocean from 1991 to 2011. *Ocean Science*, *9*(6), 1015–1055. https://doi.org/10.5194/os-9-1015-2013

Krishfield, R., Toole, J., Proshutinsky, A., & Timmermans, M.-L. (2008). Automated ice-tethered profilers for seawater observations under pack ice in all seasons. *Journal of Atmospheric and Oceanic Technology*, *25*(11), 2091–2105. https://doi.org/10.1175/2008JTECHO587.1

Krumpen, T., Belter, H. J., Boetius, A., Damm, E., Haas, C., Hendricks, S., et al. (2019). Arctic warming interrupts the Transpolar Drift and affects long-range transport of sea ice and ice-rafted matter. *Scientific Reports*, *9*(1), 5459. https://doi.org/10.1038/s41598-019-41456-y

Ksionzek, K. B., Zhang, J., Ludwichowski, K.-U., Wilhelms-Dick, D., Trimborn, S., Jendrossek, T., et al. (2018). Stoichiometry, polarity, and organometallics in solid-phase extracted dissolved organic matter of the Elbe-Weser estuary. *PLoS One*, *13*(9), e0203260. https://doi.org/10.1371/journal.pone.0203260

Lancelot, C. (1979). Gross excretion rates of natural marine phytoplankton and heterotrophic uptake of excreted products in the southern north sea, as determined by short-term kinetics. *Marine Ecology Progress Series*, *1*, 179–186. https://doi.org/10.3354/meps001179

Lawaetz, A. J., & Stedmon, C. A. (2009). Fluorescence intensity calibration using the Raman scatter peak of water. *Applied Spectroscopy*, *63*(8), 936–940. https://doi.org/10.1366/000370209788964548

Lin, H., & Guo, L. (2020). Variations in colloidal DOM composition with molecular weight within individual water samples as characterized by Flow field-flow fractionation and EEM-PARAFAC analysis. *Environmental Science & Technology*, *54*(3), 1657–1667. https://doi.org/10.1021/acs.est.9b07123

Logvinova, C. L., Frey, K. E., & Cooper, L. W. (2016). The potential role of sea ice melt in the distribution of chromophoric dissolved organic matter in the Chukchi and Beaufort Seas. *Deep Sea Research Part II: Topical Studies in Oceanography*, *130*, 28–42. https://doi.org/10.1016/j.dsr2.2016.04.017

Lund-Hansen, L. C., Markager, S., Hancke, K., Stratmann, T., Rysgaard, S., Ramløv, H., & Sorrell, B. K. (2015). Effects of sea-ice light attenuation and CDOM absorption in the water below the Eurasian sector of central Arctic Ocean (>88°N). *Polar Research*, *34*(1), 23978. https://doi.org/10.3402/polar.v34.23978

Macdonald, R. W., Harner, T., & Fyfe, J. (2005). Recent climate change in the Arctic and its impact on contaminant pathways and interpretation of temporal trend data. *The Science of the Total Environment*, *342*(1–3), 5–86. https://doi.org/10.1016/j.scitotenv.2004.12.059

Mann, P. J., Spencer, R. G. M., Hernes, P. J., Six, J., Aiken, G. R., Tank, S. E., et al. (2016). Pan-Arctic trends in terrestrial dissolved organic matter from optical measurements. *Frontiers in Earth Science*, *4*, 25. https://doi.org/10.3389/feart.2016.00025

Mathis, J. T., Hansell, D. A., Kadko, D., Bates, N. R., & Cooper, L. W. (2007). Determining net dissolved organic carbon production in the hydrographically complex western Arctic Ocean. *Limnology & Oceanography*, *52*(5), 1789–1799. https://doi.org/10.4319/lo.2007.52.5.1789

Matsuoka, A., Hill, V., Huot, Y., Babin, M., & Bricaud, A. (2011). Seasonal variability in the light absorption properties of western Arctic waters: Parameterization of the individual components of absorption for ocean color applications. *Journal of Geophysical Research*, *116*(C2), C02007. https://doi.org/10.1029/2009JC005594

Mauritzen, C. (2012). Arctic freshwater. *Nature Geoscience*, *5*(3), 162–164. https://doi.org/10.1038/ngeo1409

McKnight, D. M., Boyer, E. W., Westerhoff, P. K., Doran, P. T., Kulbe, T., & Andersen, D. T. (2001). Spectrofluorometric characterization of dissolved organic matter for indication of precursor organic material and aromaticity. *Limnology & Oceanography*, *46*(1), 38–48. https://doi.org/10.4319/lo.2001.46.1.0038

Mellat, M., Meyer, H., Brunello, C. F., Werner, M., Dahlke, S., Sommerfeld, A., et al. (2022). Stable water isotopes of underway seawater during MOSAiC expedition [Dataset]. *PANGAEA*. https://doi.org/10.1594/PANGAEA.948291

Meyer, A., Sundfjord, A., Fer, I., Provost, C., Villacieros Robineau, N., Koenig, Z., et al. (2017). Winter to summer oceanographic observations in the Arctic Ocean north of Svalbard. *Journal of Geophysical Research: Oceans*, *122*(8), 6218–6237. https://doi.org/10.1002/2016JC012391

Morris, D. P., Zagarese, H., Williamson, C. E., Balseiro, E. G., Hargreaves, B. R., Modenutti, B., et al. (1995). The attenuation of solar UV radiation in lakes and the role of dissolved organic carbon. *Limnology & Oceanography*, *40*(8), 1381–1391. https://doi.org/10.4319/lo.1995.40.8.1381

Murphy, K. R., Hambly, A., Singh, S., Henderson, R. K., Baker, A., Stuetz, R., & Khan, S. J. (2011). Organic matter fluorescence in municipal water recycling Schemes: Toward a Unified PARAFAC model. *Environmental Science & Technology*, *45*(7), 2909–2916. https://doi.org/10.1021/es103015e

Murphy, K. R., Stedmon, C. A., Graeber, D., & Bro, R. (2013). Fluorescence spectroscopy and multi-way techniques. PARAFAC. *Analytical Methods*, *5*(23), 6557–6566. https://doi.org/10.1039/c3ay41160e

Murphy, K. R., Stedmon, C. A., Waite, T. D., & Ruiz, G. M. (2008). Distinguishing between terrestrial and autochthonous organic matter sources in marine environments using fluorescence spectroscopy. *Marine Chemistry*, *108*(1–2), 40–58. https://doi.org/10.1016/j.marchem.2007.10.003

Mysak, L. A. (2001). Patterns of Arctic circulation. *Science*, *293*(5533), 1269–1270. https://doi.org/10.1126/science.1064217

Nagata, T., Fukuda, H., Fukuda, R., & Koike, I. (2000). Bacterioplankton distribution and production in deep Pacific waters: Large-scale geographic variations and possible coupling with sinking particle fluxes. *Limnology & Oceanography*, *45*(2), 426–435. https://doi.org/10.4319/lo.2000.45.2.0426

Nelson, N. B., & Siegel, D. A. (2013). The global distribution and dynamics of chromophoric dissolved organic matter. *Annual Review of Marine Science*, *5*(1), 447–476. https://doi.org/10.1146/annurev-marine-120710-100751

Nixdorf, U., Dethloff, K., Rex, M., Shupe, M., Sommerfeld, A., Perovich, D. K., et al. (2021). MOSAiC Extended Acknowledgement. *Zenodo*. https://doi.org/10.5281/zenodo.5541624

Nummelin, A., Ilicak, M., Li, C., & Smedsrud, L. H. (2016). Consequences of future increased Arctic runoff on Arctic Ocean stratification, circulation, and sea ice cover. *Journal of Geophysical Research: Oceans*, *121*(1), 617–637. https://doi.org/10.1002/2015JC011156

O'Donnell, J. A., Aiken, G. R., Swanson, D. K., Panda, S., Butler, K. D., & Baltensperger, A. P. (2016). Dissolved organic matter composition of Arctic rivers: Linking permafrost and parent material to riverine carbon. *Global Biogeochemical Cycles*, *30*(12), 1811–1826. https://doi.org/10.1002/2016GB005482

Opsahl, S., Benner, R., & Amon, R. M. W. (1999). Major flux of terrigenous dissolved organic matter through the Arctic Ocean. *Limnology & Oceanography*, *44*(8), 2017–2023. https://doi.org/10.4319/lo.1999.44.8.2017

Östlund, H. G., & Hut, G. (1984). Arctic Ocean water mass balance from isotope data. *Journal of Geophysical Research*, *89*(C4), 6373–6381. https://doi.org/10.1029/JC089iC04p06373

Paffrath, R., Laukert, G., Bauch, D., van der Loeff, M. R., & Pahnke, K. (2021). Separating individual contributions of major Siberian Rivers in the transpolar drift of the Arctic Ocean. *Scientific Reports*, *11*(1), 8216. https://doi.org/10.1038/s41598-021-86948-y

Painter, S. C., Lapworth, D. J., Woodward, E. M. S., Kroeger, S., Evans, C. D., Mayor, D. J., & Sanders, R. J. (2018). Terrestrial dissolved organic matter distribution in the North Sea. *The Science of the Total Environment*, *630*, 630–647. https://doi.org/10.1016/j.scitotenv.2018.02.237

Parlanti, E., Wörz, K., Geoffroy, L., & Lamotte, M. (2000). Dissolved organic matter fluorescence spectroscopy as a tool to estimate biological activity in a coastal zone submitted to anthropogenic inputs. *Organic Geochemistry*, *31*(12), 1765–1781. https://doi.org/10.1016/S0146-6380(00)00124-8

Pavlov, A. K., Granskog, M. A., Stedmon, C. A., Ivanov, B. V., Hudson, S. R., & Falk-Petersen, S. (2015). Contrasting optical properties of surface waters across the Fram Strait and its potential biological implications. *Journal of Marine Systems*, *143*, 62–72. https://doi.org/10.1016/j.jmarsys.2014.11.001

Pavlov, A. K., Kauko, H., Stedmon, C., & Granskog, M. (2016). N-ICE2015 colored dissolved organic matter absorption spectra [Dataset]. *PANGAEA*. https://doi.org/10.21334/npolar.2017.f46970ba

Pavlov, A. K., Stedmon, C. A., Semushin, A. V., Martma, T., Ivanov, B. V., Kowalczuk, P., & Granskog, M. A. (2016). Linkages between the circulation and distribution of dissolved organic matter in the White Sea, Arctic Ocean. *Continental Shelf Research*, *119*, 1–13. https://doi.org/10.1016/j.csr.2016.03.004

Pavlov, A. K., Taskjelle, T., Kauko, H. M., Hamre, B., Hudson, S. R., Assmy, P., et al. (2017). Altered inherent optical properties and estimates of the underwater light field during an Arctic under-ice bloom of Phaeocystis pouchetii. *Journal of Geophysical Research: Oceans*, *122*(6), 4939–4961. https://doi.org/10.1002/2016JC012471

Pegau, W. S. (2002). Inherent optical properties of the central Arctic surface waters. *Journal of Geophysical Research*, *107*(C10), 8035. https://doi.org/10.1029/2000JC000382

Polyakov, I. V., Pnyushkov, A. V., Rember, R., Padman, L., Carmack, E. C., & Jackson, J. M. (2013). Winter convection transports Atlantic water heat to the surface layer in the eastern Arctic Ocean. *Journal of Physical Oceanography*, *43*(10), 2142–2155. https://doi.org/10.1175/JPO-D-12-0169.1

Popova, E. E., Yool, A., Coward, A. C., Dupont, F., Deal, C., Elliott, S., et al. (2012). What controls primary production in the Arctic Ocean? Results from an intercomparison of five general circulation models with biogeochemistry. *Journal of Geophysical Research*, *117*(C8), C00D12. https://doi.org/10.1029/2011JC007112

Pucher, M., Wünsch, U., Weigelhofer, G., Murphy, K., Hein, T., & Graeber, D. (2019). staRdom: Versatile software for analyzing spectroscopic data of dissolved organic matter in R. *Water*, *11*, 2366. https://doi.org/10.3390/w11112366

Rabe, B., Heuzé, C., Regnery, J., Aksenov, Y., Allerholt, J., Athanase, M., et al. (2022). Overview of the MOSAiC expedition: Physical oceanography. *Elementa: Science of the Anthropocene*, *10*(1), 00062. https://doi.org/10.1525/elementa.2021.00062

Rudels, B. (1989). The formation of polar surface water, the ice export and the exchanges through the Fram Strait. *Progress in Oceanography*, *22*(3), 205–248. https://doi.org/10.1016/0079-6611(89)90013-X

Rudels, B. (2009). *Arctic Ocean circulation*. Academic Press. https://doi.org/10.1016/B978-012374473-9.00601-9

Rudels, B., Anderson, L. G., & Jones, E. P. (1996). Formation and evolution of the surface mixed layer and halocline of the Arctic Ocean. *Journal of Geophysical Research*, *101*(C4), 8807–8821. https://doi.org/10.1029/96JC00143

Rudels, B., Jones, E. P., Schauer, U., & Eriksson, P. (2004). Atlantic sources of the Arctic Ocean surface and halocline waters. *Polar Research*, *23*(2), 181–208. https://doi.org/10.1111/j.1751-8369.2004.tb00007.x

Rudels, B., Korhonen, M., Schauer, U., Pisarev, S., Rabe, B., & Wisotzki, A. (2015). Circulation and transformation of Atlantic water in the Eurasian Basin and the contribution of the Fram Strait inflow branch to the Arctic Ocean heat budget. *Progress in Oceanography*, *132*, 128–152. https://doi.org/10.1016/j.pocean.2014.04.003

Sauzède, R., Lavigne, H., Claustre, H., Uitz, J., Schmechtig, C., D'Ortenzio, F., et al. (2015). Vertical distribution of chlorophyll a concentration and phytoplankton community composition from in situ fluorescence profiles: A first database for the global ocean. *Earth System Science Data*, *7*(2), 261–273. https://doi.org/10.5194/essd-7-261-2015

Schulz, K., Koenig, Z., Muilwijk, M., Bauch, D., Clara, J., Hoppe, M., et al. (2023). The Eurasian Arctic Ocean along the MOSAiC drift (2019-2020): An interdisciplinary perspective on properties and processes. *Elementa: Science of the Anthropocene*. (Preprint). https://doi.org/10.31223/X5TT2W

Sherr, B. F., & Sherr, E. B. (2003). Community respiration/production and bacterial activity in the upper water column of the central Arctic Ocean. *Deep Sea Research Part I: Oceanographic Research Papers*, *50*(4), 529–542. https://doi.org/10.1016/S0967-0637(03)00030-X

Shupe, M. D., Rex, M., Blomquist, B., Persson, P. O. G., Schmale, J., Uttal, T., et al. (2022). Overview of the MOSAiC expedition: Atmosphere. *Elementa: Science of the Anthropocene*, *10*(1). https://doi.org/10.1525/elementa.2021.00060

Slagter, H. A., Reader, H. E., Rijkenberg, M. J. A., van der Loeff, M. R., de Baar, H. J. W., & Gerringa, L. J. A. (2017). Organic Fe speciation in the Eurasian basins of the Arctic Ocean and its relation to terrestrial DOM. *Marine Chemistry*, *197*, 11–25. https://doi.org/10.1016/j.marchem.2017.10.005

Smethie, W. M., Chipman, D. W., Swift, J. H., & Koltermann, K. P. (1988). Chlorofluoromethanes in the Arctic mediterranean seas: Evidence for formation of bottom water in the Eurasian Basin and deep-water exchange through Fram Strait. *Deep-Sea Research, Part A: Oceanographic Research Papers*, *35*(3), 347–369. https://doi.org/10.1016/0198-0149(88)90015-5

Smith, J. N., Karcher, M., Casacuberta, N., Williams, W. J., Kenna, T., & Smethie, W. M. (2021). A changing Arctic Ocean: How measured and modeled 129 I distributions indicate fundamental shifts in circulation between 1994 and 2015. *Journal of Geophysical Research: Oceans*, *126*(3), e2020JC016740. https://doi.org/10.1029/2020JC016740

Spencer, R. G. M., Aiken, G. R., Butler, K. D., Dornblaser, M. M., Striegl, R. G., & Hernes, P. J. (2009). Utilizing chromophoric dissolved organic matter measurements to derive export and reactivity of dissolved organic carbon exported to the Arctic Ocean: A case study of the Yukon River, Alaska. *Geophysical Research Letters*, *36*(6), L06401. https://doi.org/10.1029/2008GL036831

Spencer, R. G. M., Aiken, G. R., Wickland, K. P., Striegl, R. G., & Hernes, P. J. (2008). Seasonal and spatial variability in dissolved organic matter quantity and composition from the Yukon River basin, Alaska. *Global Biogeochemical Cycles*, *22*(4), GB4002. https://doi.org/10.1029/2008GB003231

Spencer, R. G. M., Mann, P. J., Dittmar, T., Eglinton, T. I., McIntyre, C., Holmes, R. M., et al. (2015). Detecting the signature of permafrost thaw in Arctic rivers. *Geophysical Research Letters*, *42*(8), 2830–2835. https://doi.org/10.1002/2015GL063498

Stedmon, C. A., Amon, R. M. W., Bauch, D., Bracher, A., Gonçalves-Araujo, R., Hoppmann, M., et al. (2021). Insights into water mass origins in the central Arctic Ocean from in-situ dissolved organic matter fluorescence. *Journal of Geophysical Research: Oceans*, *126*(7), e2021JC017407. https://doi.org/10.1029/2021JC017407

Stedmon, C. A., Amon, R. M. W., Rinehart, A. J., & Walker, S. A. (2011). The supply and characteristics of colored dissolved organic matter (CDOM) in the Arctic Ocean: Pan Arctic trends and differences. *Marine Chemistry*, *124*(1–4), 108–118. https://doi.org/10.1016/j.marchem.2010.12.007

Stedmon, C. A., Granskog, M. A., & Dodd, P. A. (2015). An approach to estimate the freshwater contribution from glacial melt and precipitation in East Greenland shelf waters using colored dissolved organic matter (CDOM). *Journal of Geophysical Research: Oceans*, *120*(2), 1107–1117. https://doi.org/10.1002/2014JC010501

Stedmon, C. A., & Markager, S. (2001). The optics of chromophoric dissolved organic matter (CDOM) in the Greenland Sea: An algorithm for differentiation between marine and terrestrially derived organic matter. *Limnology & Oceanography*, *46*(8), 2087–2093. https://doi.org/10.4319/lo.2001.46.8.2087

Stedmon, C. A., Markager, S., & Bro, R. (2003). Tracing dissolved organic matter in aquatic environments using a new approach to fluorescence spectroscopy. *Marine Chemistry*, *82*(3–4), 239–254. https://doi.org/10.1016/S0304-4203(03)00072-0

Stedmon, C. A., & Nelson, N. B. (2015). The optical properties of DOM in the Ocean. In *Biogeochemistry of marine dissolved organic matter (Academic P)* (pp. 481–508). Elsevier. https://doi.org/10.1016/B978-0-12-405940-5.00010-8

Stedmon, C. A., Thomas, D. N., Granskog, M., Kaartokallio, H., Papadimitriou, S., & Kuosa, H. (2007). Characteristics of dissolved organic matter in Baltic coastal sea ice: Allochthonous or autochthonous origins? *Environmental Science & Technology*, *41*(21), 7273–7279. https://doi.org/10.1021/es071210f

Terhaar, J., Lauerwald, R., Regnier, P., Gruber, N., & Bopp, L. (2021). Around one third of current Arctic Ocean primary production sustained by rivers and coastal erosion. *Nature Communications*, *12*(1), 169. https://doi.org/10.1038/s41467-020-20470-z

Tippenhauer, S., Vredenborg, M., Heuzé, C., Ulfsbo, A., Rabe, B., Granskog, M. A., et al. (2023a). Physical oceanography based on Ocean City CTD during POLARSTERN cruise PS122 [Dataset]. *PANGAEA*. https://doi.org/10.1594/PANGAEA.959964

Tippenhauer, S., Vredenborg, M., Heuzé, C., Ulfsbo, A., Rabe, B., Granskog, M. A., et al. (2023b). Physical oceanography based on ship CTD during POLARSTERN cruise PS122 [Dataset]. *PANGAEA*. https://doi.org/10.1594/PANGAEA.959963

Tippenhauer, S., Vredenborg, M., Heuzé, C., Ulfsbo, A., Rabe, B., Granskog, M. A., et al. (2023c). Physical oceanography water bottle samples based on Ocean City CTD during POLARSTERN cruise PS122 [Dataset]. *PANGAEA*. https://doi.org/10.1594/PANGAEA.959966

Tippenhauer, S., Vredenborg, M., Heuzé, C., Ulfsbo, A., Rabe, B., Granskog, M. A., et al. (2023d). Physical oceanography water bottle samples based on ship CTD during POLARSTERN cruise PS122 [Dataset]. *PANGAEA*. https://doi.org/10.1594/PANGAEA.959965

Toole, J., Krishfield, R., Timmermans, M.-L., & Proshutinsky, A. (2011). The ice-tethered profiler: Argo of the Arctic. *Oceanography*, *24*(3), 126–135. https://doi.org/10.5670/oceanog.2011.64

Tremblay, J.-É., & Gagnon, J. (2009). The effects of irradiance and nutrient supply on the productivity of Arctic waters: A perspective on climate change. In J. C. J. Nihoul & A. G. Kostianoy (Eds.), *Influence of climate change on the changing Arctic and Sub-Arctic conditions* (pp. 73–93). Springer Netherlands. https://doi.org/10.1007/978-1-4020-9460-6_7

Underwood, G. J. C., Michel, C., Meisterhans, G., Niemi, A., Belzile, C., Witt, M., et al. (2019). Organic matter from Arctic sea-ice loss alters bacterial community structure and function. *Nature Climate Change*, *9*(2), 170–176. https://doi.org/10.1038/s41558-018-0391-7

Wagner, S., Jaffé, R., Cawley, K., Dittmar, T., & Stubbins, A. (2015). Associations between the molecular and optical properties of dissolved organic matter in the Florida Everglades, a model coastal Wetland system. *Frontiers in Chemistry*, *3*, 66. https://doi.org/10.3389/fchem.2015.00066

Walker, S. A., Amon, R. M. W., & Stedmon, C. A. (2013). Variations in high-latitude riverine fluorescent dissolved organic matter: A comparison of large Arctic rivers. *Journal of Geophysical Research: Biogeosciences*, *118*(4), 1689–1702. https://doi.org/10.1002/2013JG002320

Weishaar, J. L., Aiken, G. R., Bergamaschi, B. A., Fram, M. S., Fujii, R., & Mopper, K. (2003). Evaluation of specific ultraviolet absorbance as an indicator of the chemical composition and reactivity of dissolved organic carbon. *Environmental Science & Technology*, *37*(20), 4702–4708. https://doi.org/10.1021/es030360x

Wetzel, R. G. (1984). Detrital dissolved and particulate organic carbon functions in aquatic ecosystems. *Bulletin of Marine Science*, *35*, 503–509.

Wünsch, U. J., Bro, R., Stedmon, C. A., Wenig, P., & Murphy, K. R. (2019). Emerging patterns in the global distribution of dissolved organic matter fluorescence. *Analytical Methods*, *11*(7), 888–893. https://doi.org/10.1039/c8ay02422g

Yamashita, Y., & Jaffé, R. (2008). Characterizing the interactions between trace metals and dissolved organic matter using excitation−emission matrix and parallel factor analysis. *Environmental Science & Technology*, *42*(19), 7374–7379. https://doi.org/10.1021/es801357h

Zabłocka, M., Kowalczuk, P., Meler, J., Peeken, I., Dragańska-Deja, K., & Winogradow, A. (2020). Compositional differences of fluorescent dissolved organic matter in Arctic Ocean spring sea ice and surface waters north of Svalbard. *Marine Chemistry*, *227*, 103893. https://doi.org/10.1016/j.marchem.2020.103893